SAND90–1162 • UC–236
Unlimited Release
Printed October 1991

C.2

Characteristics, Finite Element Analysis, Test Description, and Preliminary Test Results of the STM4-120 Kinematic Stirling Engine

Kevin L. Linker, K. Scott Rawlinson, Gregory Smith

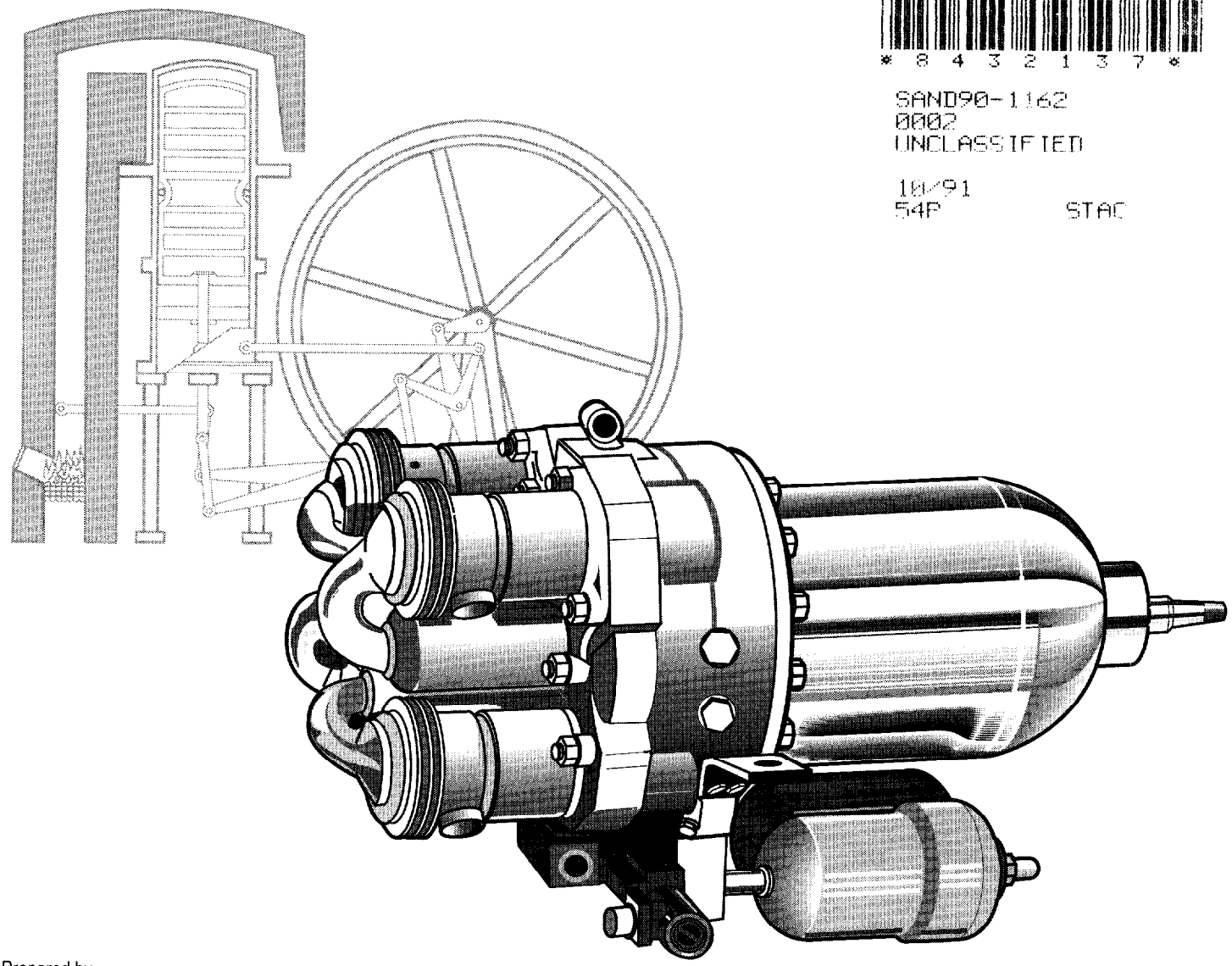

Prepared by
Sandia National Laboratories
Albuquerque, New Mexico 87185 and Livermore, California 94550
for the United States Department of Energy
under Contract DE-AC04-76DP00789

Issued by Sandia National Laboratories, operated for the United States Department of Energy by Sandia Corporation.

Available to DOE and DOE contractors from
Office of Scientific and Technical Information
PO Box 62
Oak Ridge, TN 37831

Prices available from (615) 576-8401, FTS 626-8401

Available to the public from
National Technical Information Service
US Department of Commerce
5285 Port Royal Rd
Springfield, VA 22161

NTIS price codes
Printed copy: A03
Microfiche copy: A01

SAND90-1162
Unlimited Release
Printed October 1991

Distribution
Category UC-236

CHARACTERISTICS, FINITE ELEMENT ANALYSIS, TEST DESCRIPTION, AND PRELIMINARY TEST RESULTS OF THE STM4-120 KINEMATIC STIRLING ENGINE*

Kevin L. Linker
Solar Thermal Electric Technology

K. Scott Rawlinson
Gregory Smith
Solar Thermal Test Facility

Sandia National Laboratories
Albuquerque, New Mexico 87185

ABSTRACT

The Department of Energy's Solar Thermal Program has as one of its program elements the development and evaluation of conversion device technologies applicable to dish-electric systems. The primary research and development combines a conversion device (heat engine), solar receiver, and generator mounted at the focus of a parabolic dish concentrator. The Stirling-cycle heat engine was identified as the conversion device for dish-electric with the most potential for meeting the program's goals for efficiency, reliability, and installed cost. To advance the technology toward commercialization, Sandia National Laboratories has acquired a Stirling Thermal Motors, Inc., kinematic Stirling engine, STM4-120, for evaluation. The engine is being bench-tested at Sandia's Engine Test Facility and will be combined later with a solar receiver for on-sun evaluation. This report presents the engine characteristics, finite element analyses of critical engine components, test system layout, instrumentation, and preliminary performance results from the bench test.

*This work was supported by the U.S. Department of Energy under Contract DE-AC04-76DP00789.

ACKNOWLEDGEMENTS

The authors would like to thank Vern Dudley, Daniel Ray, Walt Einhorn, Tim Moss, and Ted Bryant for their help during the past year on the STM4-120 kinematic Stirling Engine project. In addition, the authors would like to extend their thanks to those at Stirling Thermal Motors, Inc., who have contributed along the way.

Cover: Artists' renditions of the original Stirling engine patent of 1816 and today's STM4-120 Stirling engine.

FOREWORD

The research and development program described in this document was conducted within the U.S. Department of Energy's Solar Thermal Technology Program to advance the engineering and scientific understanding of solar thermal technology, and to establish the technology base from which private industry can develop solar thermal power production options for the competitive energy market.

Solar thermal technology concentrates solar radiation with tracking mirrors or lenses onto a receiver where the solar energy is absorbed as heat and then converted into electricity or incorporated into products as process heat. The two primary solar thermal technologies, central receivers and distributed receivers, employ various point and line-focus optics to concentrate sunlight. Current central receiver systems use fields of heliostats (two-axis tracking mirrors) to focus the sun's radiant energy onto a single tower-mounted receiver. Troughs and bowls are line-focus tracking reflectors that concentrate sunlight onto receiver tubes along their focal lines. Concentrating collector modules can be used alone or in a multi-module system. The concentrated radiant energy absorbed by the solar thermal receiver is transported to the conversion process by a circulating working fluid. Receiver temperatures range from 100°C in low-temperature troughs to over 1500°C in dish and central receiver systems.

The Solar Thermal Technology Program directs efforts to advance and improve promising system concepts through research and development of solar thermal materials, components, and subsystems, and testing and performance evaluation of subsystems and systems. Under the technical direction of the Department of Energy and its network of national laboratories, which work with private industry, a comprehensive, goal-directed program to improve performance and provide technically proven options for eventual incorporation into the nation's energy supply has been established.

To contribute successfully to an adequate national energy supply at reasonable cost, solar thermal energy must eventually be economically competitive with a variety of other energy sources. Components and system-level performance targets have been developed as quantitative program goals used in planning research and development activities, measuring progress, assessing alternative technology options, and developing components. This report outlines performance characteristics of the Stirling Thermal Motors STM4-120 kinematic Stirling engine. It is believed that this engine has the greatest near-term potential for meeting the Department of Energy's commercialization goals for distributed-receiver solar-electric systems.

CONTENTS

FIGURES

Page

FIGURES (Continued)

Page

TABLES

I. INTRODUCTION

Since its development in 1816 by Dr. Robert Stirling, the Stirling-cycle heat engine (hereafter referred to as Stirling engine) has been considered for many practical applications including solar thermal energy. In 1872, John Ericsson constructed a small "Stirling Cycle Sun Motor" utilizing a parabolic reflector to collect and concentrate solar energy to a Stirling engine [1]. Since then, advances in materials and the ability to analyze the Stirling engine theoretically have made it a serious contender for solar applications. Stirling engines have several excellent qualities for solar thermal systems, including high conversion efficiencies of 30 to 45%; a completely closed cycle that provides potential for extended life; high specific power, implying reduced weight at focal point of a parbolic dish; quiet and benign operation, which allows their installation in inhabited areas; and external heating, which permits hybrid operation fossil fuel and solar energy [2].

In the Department of Energy (DOE)-funded Vanguard project, a Stirling engine was mounted at the focus of a parabolic dish and successfully demonstrated a system (concentrator, collector, and engine) net solar-to-electric conversion efficiency of 29.4% [3,4]. The Stirling engine used was a four-cylinder United Stirling (USAB) model 4-95, kinematic automotive engine, modified for solar applications. Its design life before overhaul was 3,500 hours, but a solar application requires at least 60,000 hours to meet DOE's levelized energy costs goals of $.05/kWh. The major life limitation of the 4-95 was the mechanical hardware such as the drive mechanism and piston rod seals. In addition, the directly illuminated heater heads demanded an accurate and costly concentrator. An equal solar flux was required on each of four heater heads for high cycle efficiency and engine life. Finally, the power control system was very complex, requiring considerable hardware to change the pressure of the hydrogen working fluid. Because of these modifications, the USAB 4-95 was not considered a reliable long-term system. Thus, DOE's Solar Thermal Electric Program searched for a Stirling engine to meet the requirements for reliability, life, and performance for a dish-electric system, and has concluded that the Stirling Thermal Motors (STM), STM4-120, kinematic Stirling engine may well meet these requirements [5,6].

Sandia National Laboratories (SNL), the DOE's lead laboratory for solar thermal-electric systems research, has procured an STM4-120 for bench-testing at SNL's Engine Test Facility (ETF) (Figure 1). Obtaining performance and reliability data is the main thrust of this testing. With Sandia's reflux solar receiver development, an eventual on-sun evaluation of an STM4-120 and reflux receiver is planned [7,8].

Figure 1. STM4-120 in ETF test cell.

Background

The Stirling engine is theoretically simple in that a closed volume of working fluid, usually helium or hydrogen gas, is alternately heated and cooled while being compressed and expanded, resulting in a net power output. Unlike an internal combustion (IC) engine, the Stirling engine is an externally heated engine. Any high-quality heat source such as fossil fuel combustion, nuclear energy, waste heat, or solar energy can operate the Stirling engine.

The Stirling engine's thermodynamics can be characterized by four distinctive endpoints as shown in the temperature-entropy (T-S) and pressure-volume (P-V) diagrams in Figure 2 (T_h refers to temperature on hot side of engine while T_c refers to cold side). This theoretical cycle can be achieved with simulated hardware arranged in a Beta engine configuration [9]. (The Beta engine configuration is one of three Stirling engine arrangements. The other two configurations are identified as an Alpha and a Gamma. The difference between all three being the arrangement of the pistons.) The engine consists of a power piston, a displacer piston, a cooler, a regenerator, and a heater all enclosed with a volume of working fluid, typically a gas. For this ideal engine, the regenerator is not shown as an active component in the cycle. In fact, the regenerator is vital to a Stirling cycle, for it contributes to its high thermal efficiency. The cycle begins with the power and displacer pistons at the outer portions of their stroke (point a). The power piston moves toward the compression space, reducing the volume of the working fluid, slightly increasing the pressure, and rejecting heat through the cooler (points a to b). This is called the isothermal compression stage. The displacer piston then moves the working fluid to the expansion space (points b to c). This stage is referred to as constant volume displacement, where the pressure and temperature of the working fluid are raised.

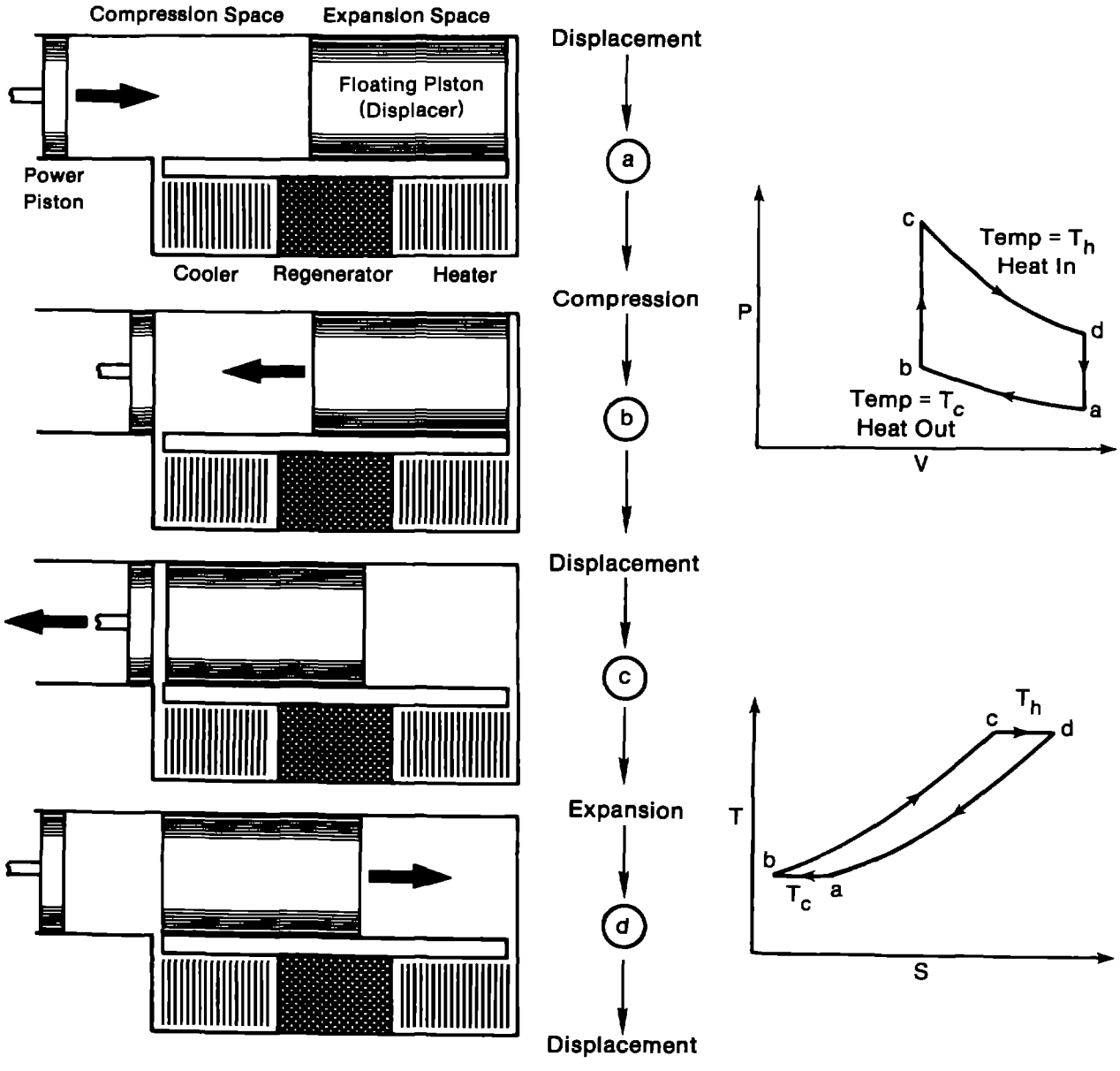

Figure 2. Stirling cycle.

In the expansion space, the addition of heat to the working fluid (points c to d) causes the gas to expand (also called isothermal expansion), driving the power piston from right-to-left. Once the gas has expanded, the displacer returns to the expansion space (points d to a) to begin the cycle again. This last stage is referred to as constant volume displacement. Net power from the cycle is obtained because the expanded gas pressure acting on the power piston is larger in its right-to-left motion than compressing the gas in its left-to-right motion. In an actual Stirling engine, the movement of the displacer and power piston and the method of extracting power are intricate functions that can be achieved by two conventional Stirling engine designs.

Stirling engines can be categorized as either kinematic or free-piston designs (Figure 3). The kinematic engine has its pistons fixed or constrained mechanically by a drive mechanism. This is similar to an internal combustion engine in that the thermodynamic work is transferred to mechanical work. A free-piston engine, on the other hand, has pistons that are free to move within the engine and are not mechanically attached to each other. Performance of the kinematic Stirling engine relies on the change in working space volume with time caused by the mechanical dynamics. The free-piston engine performance depends on the thermodynamics and mechanical dynamics and the interaction between the two.

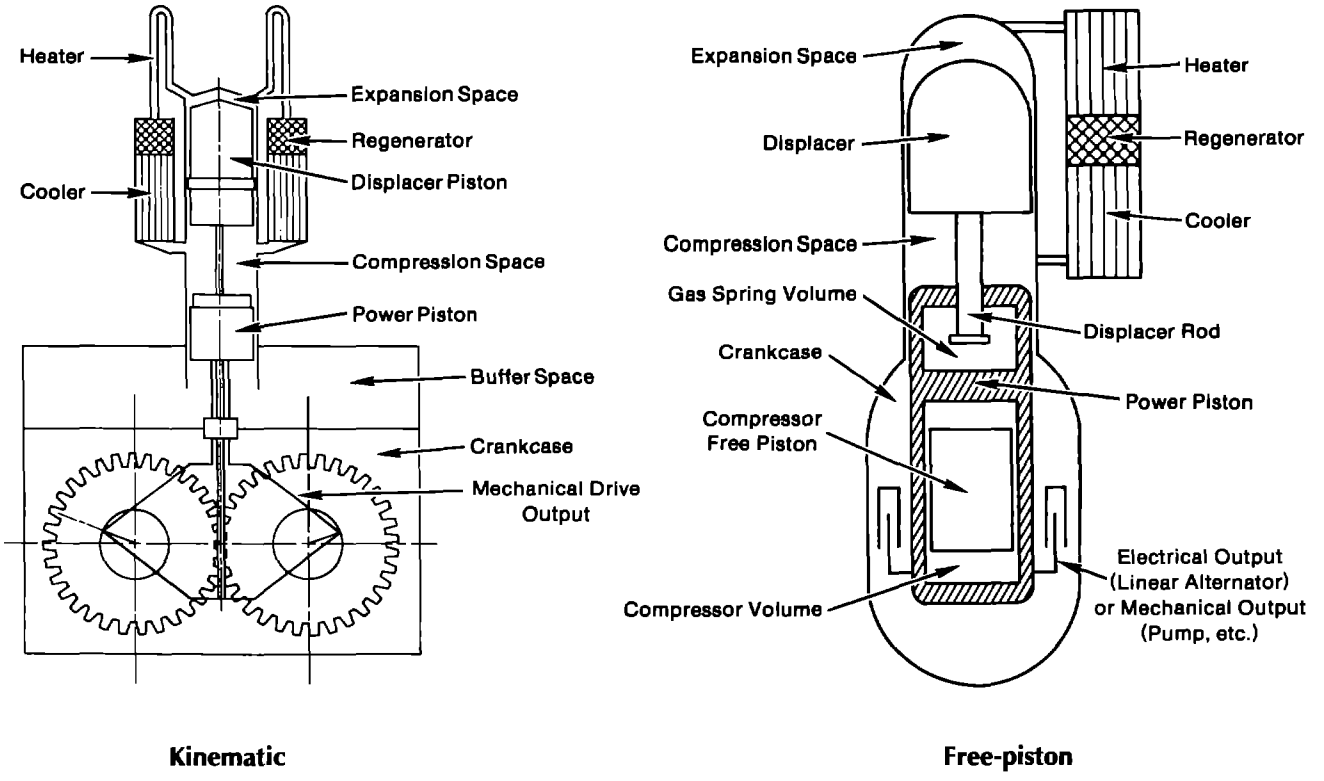

Figure 3. Kinematic versus free-piston engines.

II. CHARACTERISTICS OF STIRLING ENGINES

The Stirling engine has several attributes that make it an excellent energy conversion device [9,10]. These features include:

- High conversion efficiency. The Stirling engine has demonstrated thermal efficiencies (shaft power out divided by heat into the engine) of 30 to 45%.

- Quiet operation. Because of the external heating and the absence of valves, cams, and timing gears, etc., the Stirling engine can be extremely quiet.

- Multi-fuel capability. With external heating and a closed cycle, a Stirling engine can operate with virtually any fuel or heat source, e.g., fossil fuel, solar energy, etc.

- High power-to-weight ratio. High thermal efficiencies give the Stirling engine a high power-to-weight ratio. A Stirling engine's power-to-weight ratio is equal to that of a turbocharged diesel engine.

- Long-life operation. A closed-cycle engine such as the Stirling allows for the potential of long service lifetimes with high reliability. With hermetic sealing, the internal components of the engine would not be exposed to a harsh environment, resulting in longer life.

- Stirling engines use environmentally benign working fluids such as air, hydrogen, or helium within the cycle.

- Stirling engines have a high efficiency over a wide range of operating conditions.

The many advantages of the Stirling engine make it useful in several applications. Stirling engines have been used for heat pumps, cryocoolers, artificial heart pumps, and auxiliary power units. Most recently, the Stirling engine completed a major development program, through the DOE and National Aeronautics and Space Administration, for automotive engines. Over a 10-year period this engine was brought close to commercialization [11]. However, displacing the automotive IC engine is a difficult task. The IC engine is well developed and has a large support infrastructure, and with the increasing use of computers, it is continually improving. As a power conversion unit for renewable energy, however, the Stirling engine can be used where IC engines cannot operate.

A successful demonstration using solar energy and Stirling engines was performed in 1984 and 1985 through the DOE-funded Vanguard project. Utilizing concentrated

sunlight as the heat source, a system net electric-output to heat-input efficiency of 29.4% was achieved. To date, this is the highest recorded conversion efficiency for any solar-driven system.

Characteristics of the STM4-120

The STM4-120 kinematic Stirling engine is a four-cylinder, double-acting piston design coupled to a variable swashplate drive mechanism (Figures 4 and 5). The STM4-120 incorporates several design innovations intended to correct problems that have plagued previous Stirling engines. The following list compares the previous Stirling engine designs with the STM4-120.

Previous (e.g., USAB 4-95)	**Current** (STM4-120)
• Cycle pressure control that provides a complex method for controlling power output.	• Variable swashplate, which allows for a variable-stroke engine that is compact, reliable, and simple to control.
• Piston rod seals as both pressure seals and oil scrapers, resulting in limited life.	• Pressurized crankcase which allows piston rod seals to act only as scrapers to remove lubricating oil.
• Nonuniform heating of engine heater heads caused reliability and inefficiencies within engine.	• Heat pipe input, in which sodium heat pipes allow even heat input to the engine and flexible energy sources.

At a heater head temperature of 800°C and cooler temperature of 45°C, the engine is designed to deliver a nominal 25 kW of shaft power at full stroke (48.5 mm) and 1800 RPM. This corresponds to a design conversion efficiency, defined as shaft power out divided by heat into the engine, of 40 to 45% without auxiliaries. The STM4-120 engine has four double-acting cylinders arranged symmetrically about a common axis with one heater, regenerator, and cooler assembly serving each cylinder. Double-acting cylinders imply that the top and bottom of each piston in the cylinders are acted upon by the working fluid. Each cylinder has a 56-mm bore with a piston stroke of 48.5 mm. The engine weighs 75 kg without the heat input system, measures 635 mm in length and 300 mm in diameter, and uses helium as its working fluid. The external heating system, which operates at 800°C, uses several high-temperature alloys including XF818 (heater heads), SS316 (heater tubes), SS321/SS304 (heat pipe and evaporator), and Inconel 625 (bellows). The cold side (<100°C) of the engine utilizes more common steels and aluminum alloys.

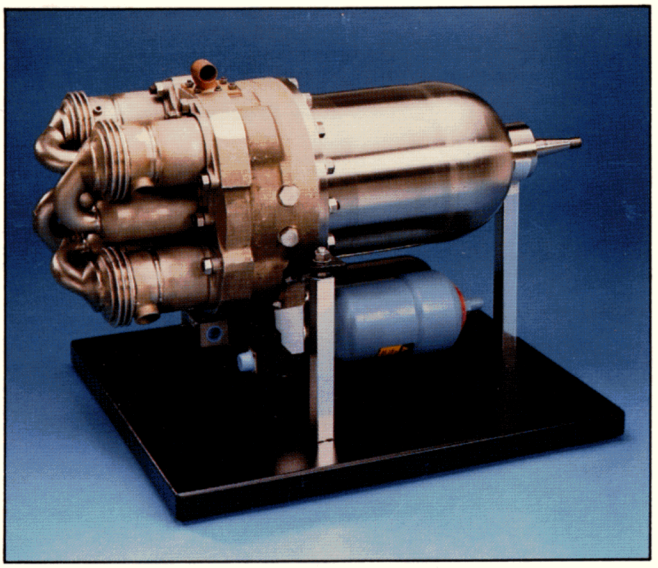

Figure 4. STM4-120 engine.

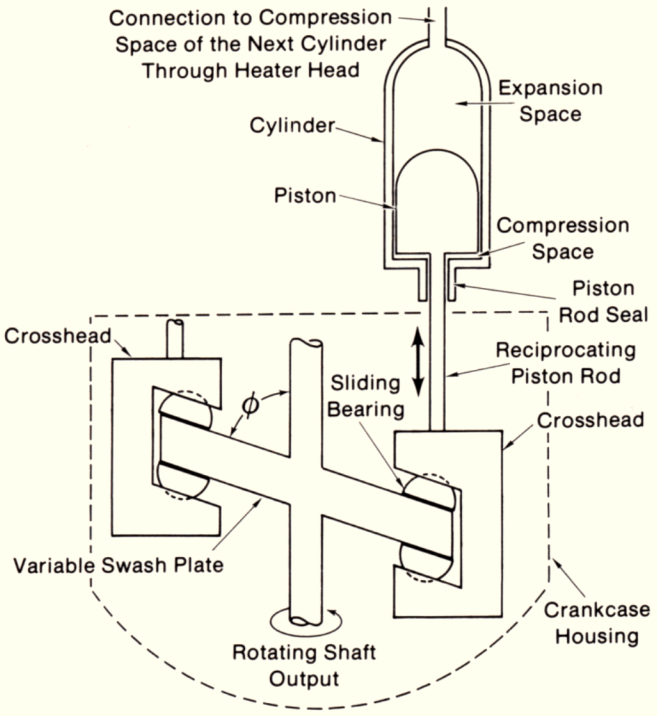

Figure 5. Schematic of an STM4-120 engine cross section.

The variable swashplate drive gives the STM4-120 compact and simple power control. Through a rotary actuator, the angle of the swashplate is changed relative to the output shaft of the engine. With the pistons connected to the perimeter of the swashplate, via a piston rod and crosshead, the piston stroke varies with the change in swashplate angle (ϕ) and can be changed from 0 to 48.5 mm. This allows for a continuous control system that is completely self-contained within the engine. In contrast, previous kinematic Stirling engines have been controlled via a pressure-control scheme that shuttled the engine working fluid into or out of the working space. A complex arrangement of valves, tubing, and a compressor (Figure 6) was required.

Piston rod seals have been a continuing source of problems limiting the reliability and life of the kinematic Stirling engine. Previous Stirling engines required the piston rod seals to scrape the crankcase lubricating oil from the piston rods and to seal the high-pressure (>10.3 MPa) gases of the working fluid from the atmospheric pressure crankcase. The ability of these seals to do two jobs at once for extended periods has been difficult to achieve. To eliminate the high-pressure sealing, the STM4-120 has been designed with a pressurized crankcase. The piston rod seals can now be designed only to separate lubricating oil from the engine cycle working fluid.

Finally, the STM4-120 uses heat pipe technology to provide energy to the engine, which allows greater flexibility in the type of heat source used for the engine. The heat pipes transfer energy from the heat source to the working fluid in the engine through a heat exchanger. The STM4-120 uses liquid sodium heat pipes. With a sodium heat pipe design, a solar receiver incorporating the engine heater heads can be constructed to "smooth out" the uneven flux distribution on the solar absorbing surface, thereby reducing the required accuracy and, subsequently, the cost of the parabolic concentrator. In addition, the heat pipes allow an equal amount of heat to be transferred into the engine's four pistons, resulting in greater efficiency and reliability.

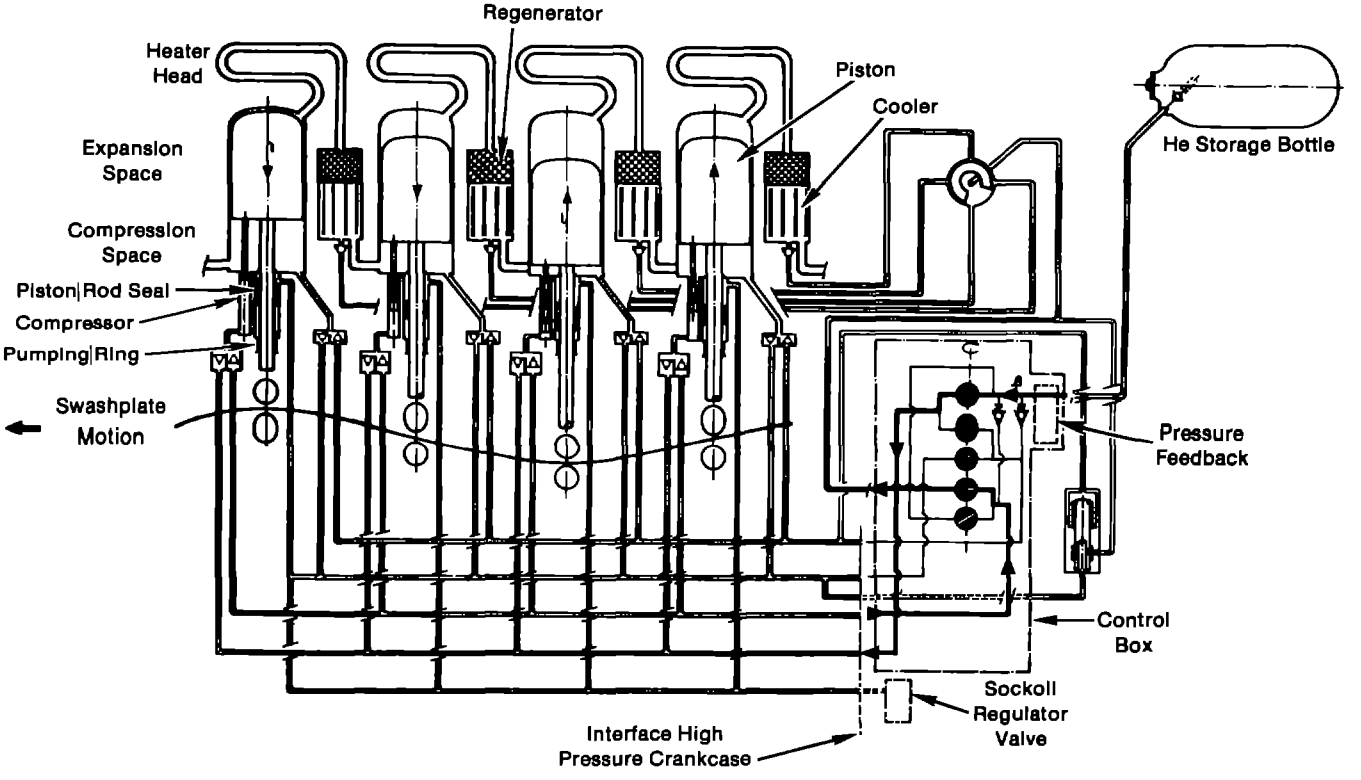

Figure 6. Typical control system for previous Stirling engines.

III. FINITE ELEMENT ANALYSIS OF CRITICAL COMPONENTS

Several critical engine components of the STM4-120 Stirling engine test program were analyzed by the authors at SNL using Finite Element Analysis (FEA) to provide an independent quality check, to eliminate reliability problems, and to ensure safe operation of the engine and heat pipes. The components analyzed were determined to be important because of their exposure to high stress and/or high temperature. Other components were chosen because testing proved them to be potentially vulnerable to failure. The components analyzed include the regenerator housing, the cylinder housing, the pressure hull and oil sump vessels, and the swashplate. Figure 7 locates each within the engine, and the components and the analysis results are discussed below.

The FEA computer code used to analyze the engine is COSMOS/M™*, which is commercially available and can be operated on a personal computer. It includes pre-processing for generating two- and three-dimensional models, and automatic mesh and volume generation. All stresses displayed and discussed below are Von Mises, a common criterion in design and failure analysis, and all displacements are in millimeters.

Regenerator Housing

The regenerator housing is a major part of the heater head assembly (see Figure 8) and houses the engine's regenerator. It endures both high pressure and extreme temperature. The bottom flange of the regenerator bolts to the engine crankcase. The top of the housing is bored out, and

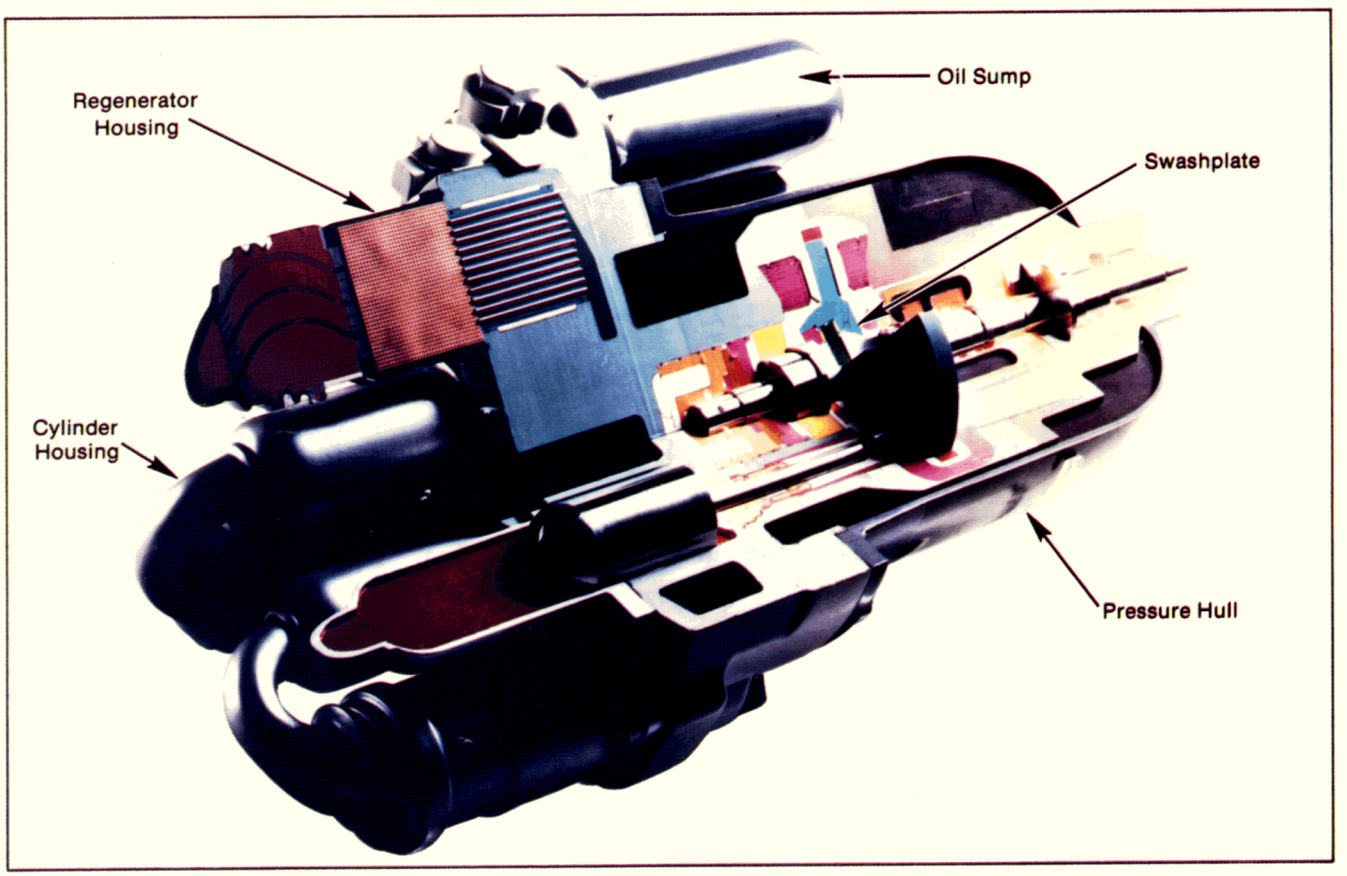

Figure 7. STM4-120 component location.

*The use of brand names in this report is for identification only, and does not imply endorsement of specific products by Sandia National Laboratories.

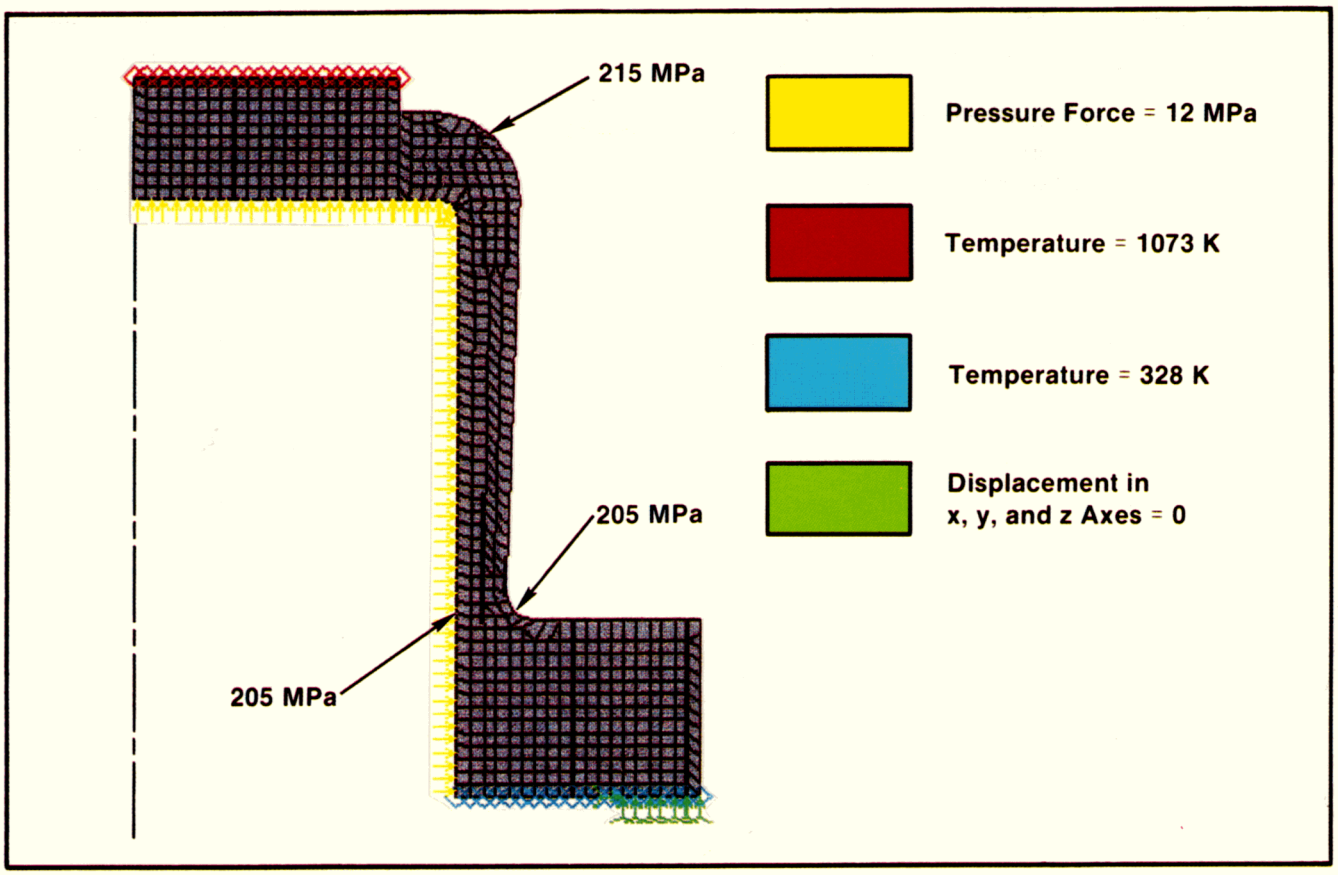

Figure 8. Regenerator element and boundary conditions.

the header plate for the heater-head tube bundle is welded into this bore. Due to the tube bundle penetrations, this plate is perforated, not solid. SNL analyzed the housing using both solid plate and perforated plate models. The perforated plate area was modeled using an adjusted value for the modulus of elasticity and Poisson's ratio to account for porosity. Although displacements between the two plates are different, high-stress areas are similar. Using an axisymmetric model, only a cross section of the component is needed. An element and boundary condition plot of the housing is shown in Figure 8. The model is summarized below:

- Element type: 4-node quadrilateral, "PLANE2D", axisymmetric;
- Average element size: 1.5 mm;
- Pressure/force boundary conditions: 12 MPa applied to all interior element faces (yellow area);
- Temperature boundary conditions: 1073 K along top heater flange surface, 328 K along bottom bolt flange surface (red and blue areas);
- Displacement boundary conditions: Zero displacement in x and y directions at centerline of bolthole pattern (58 mm from centerline), and zero y-displacement radially outward from this point (green area);
- Modulus of elasticity: 1.38×10^5 N/mm^2 with the exception of perforated plate area having a modified value of 5.5×10^4 N/mm^2;
- Poisson's ratio: 0.3, with the exception of perforated plate area having a modified value of 0.32;
- Thermal conductivity: 2.0×10^{-2} W/mm-K;
- Coefficient of thermal expansion: 17.37 µm/m-K.

Figure 9 shows the analysis results for the solid plate case. The displacement determined by the analysis yielded a maximum of 0.78 mm for the free end, mostly due to thermal expansion. The high-stress areas of interest include the outside upper radius at 215 MPa, the outside lower radius at 205 MPa, and the inner wall opposite the outside lower radius at 205 MPa.

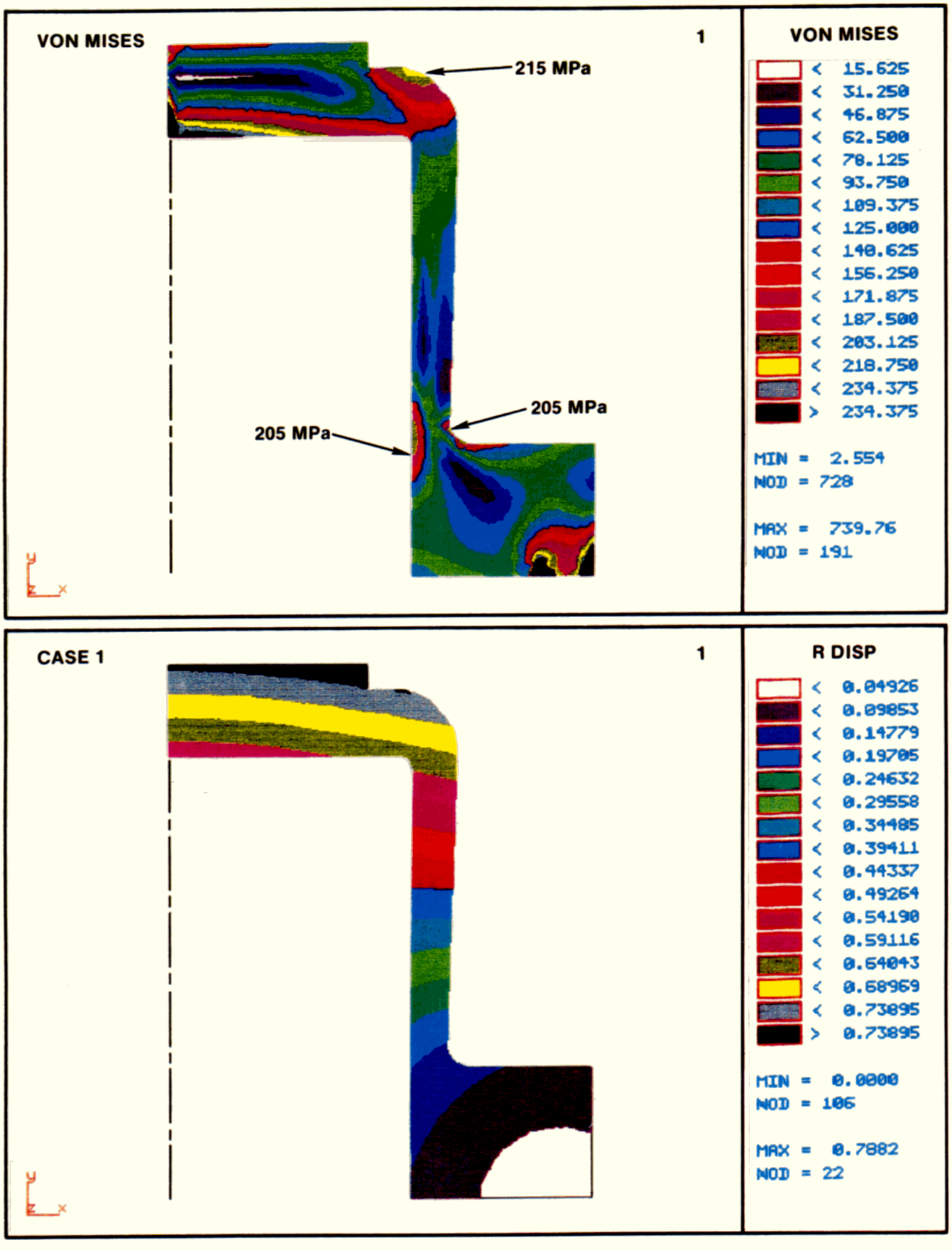

Figure 9. Regenerator stress and displacement (solid plate assumption).

Some noteworthy high stresses exist at the outside edge of the flange (Figure 9) from the severity of the boundary conditions applied. No displacement in the y-direction is allowed from the centerline of the bolthole, and radially outward from this point, and no displacement is allowed in the x-direction at the center of the bolthole. In actuality, the part that mates to the flange is not rigid and therefore will displace somewhat, relieving these local stresses. The flange is also the base for the cylinder housing. Pressure in the adjacent cylinder housing will tend to deform the flange upward and will also eliminate the high-stress area. To determine the stresses in this area, a three-dimensional detailed model of the regenerator and cylinder housing would be needed. Because (a) problems in the flange have not developed, (b) model inaccuracies explain the high-stress area, and (c) the model complexity would probably exceed the COSMOS/M™ capabilities, a three-dimensional model was not developed. Because these stresses can be attributed to approximations in the model and they occur in an area of low temperature, they can be disregarded.

The model was then modified to determine the effect of the perforated header plate. This model more closely represents the actual situation and results are presented in Figure 10. The displacement analysis yielded a maximum of 0.81 mm for the free end, again mostly because of thermal expansion. The high-stress areas of interest include the outside upper radius at 220 MPa, the outside lower radius at 220 MPa, and the inner wall opposite the outside lower radius at 205 MPa.

The upper outside radius is of concern primarily because the endurance limit of materials is much lower at high temperature. The FEA model predicts a temperature of 966 K at this point. In addition to the loading at the mean cycle pressure of 12 MPa, the regenerator housing is subjected to alternating stresses caused by cycle pressure variations, so SNL analyzed the stresses at the minimum and maximum cycle pressures of 9 and 15 MPa. Fortunately, the alternating stresses are only 10 MPa. SNL calculated the fatigue-creep life to be 9124 hours, based on an endurance limit of 105 MPa. Because the endurance limit used is very conservative, problems with the regenerator housing are not expected during prototype testing. This life will increase with future development to approach the 60,000-hour lifespan of engine [12, 13].

STM previously performed an FEA (using the same FEA code as SNL) on the regenerator housing, but the results were quite different [14]. The stresses at the outer upper radius were 132 MPa for the perforated plate model—significantly less than predicted by SNL. The reason for the discrepancies was STM's boundary conditions. The boundary conditions in the SNL model were modified, enabling SNL researchers to duplicate STM's results. In STM's analysis, the flange was allowed to displace in the x-direction, which would tend to reduce the stresses in the area of concern. Allowing the flange to float in this direction is reasonable away from the bolts, but not near bolts or adjacent to the cylinder housing. In addition, STM used slightly different temperature boundary conditions at the header plate. The SNL model is considered "worst case" relative to STM's model. The actual maximum stresses are probably between STM's and SNL's predictions. Interestingly, STM predicted a similar fatigue life because their model predicted a higher temperature at this point.

Fatigue-life is extremely sensitive to small changes in temperature. In testing the STM engine in the ETF, we have operated the engine at 780°C instead of 800°C. This 20°C change in temperature, assuming the same stress level, increases the predicted life from 9124 hours to nearly 35,000 hours.

In addition to the analyses discussed above, SNL analyzed the regenerator housing with pressure loading only and temperature loading only. The pressure loading cases produced lower stresses than did the combined temperature and pressure case. The high-stress area with pressure only was the inner upper radius (instead of the outer upper radius) of the housing at 174 MPa. This makes proof-testing of the regenerator housings difficult because the stress pattern is different with pressure only when compared to combined temperature and pressure loading. The high-stress areas for the temperature-only case included 160 MPa at the inner upper radius, and 260 MPa at the lower outside radius.

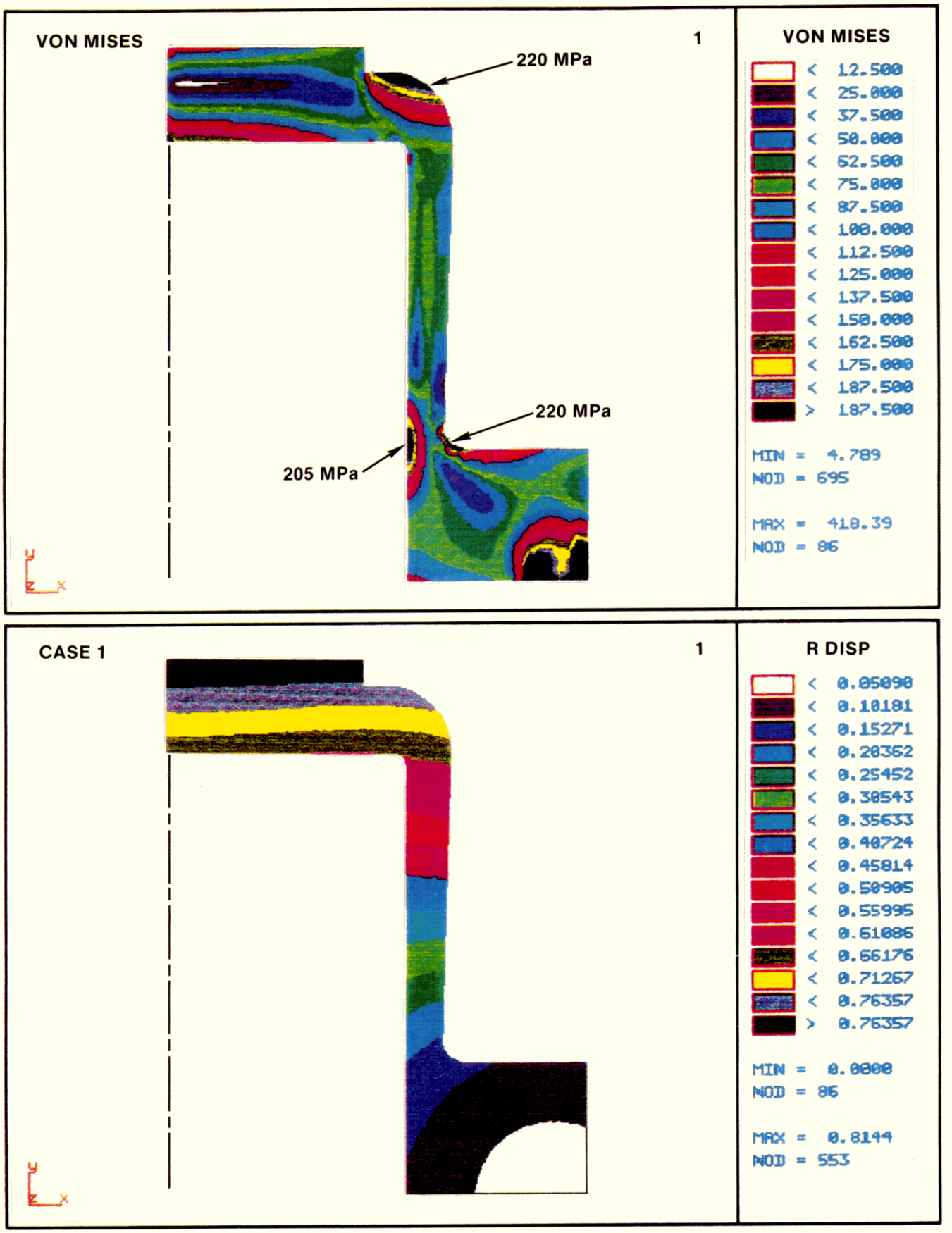

Figure 10. Regenerator stress and displacement (perforated plate assumption).

Cylinder Housing

Figure 11 displays an element and boundary condition plot of the cylinder housing cross section. The cylinder houses the piston assembly and is connected to the regenerator through a hot connecting duct attached to the top flange. The bottom flange of the part is bolted to the front crankcase. Like the regenerator housing, the cylinder housing is axisymmetric with the exception of the bottom flange, and thus the results near the bottom flange are not considered accurate. Because the bottom flange extends outside of, and is not an integral part of, the cylinder housing, the probability of high stresses in this part is questionable. The cylinder housing was modeled using the following parameters:

- Element type: 4-node quadrilateral, "PLANE2D", axisymmetric;
- Average element size: 1 mm;
- Pressure force boundary conditions: 12 MPa applied to all interior element faces (yellow area);
- Temperature boundary conditions: 1073 K along top heater flange surface, 328 K along bottom bolt flange surface (red and blue areas);
- Displacement boundary conditions: Zero displacement in x and y directions at centerline of bolthole pattern (45 mm from axis), and zero y-displacement radially outward from this point (green area);
- Modulus of elasticity: 1.38×10^5 N/mm^2;
- Poisson's ratio: 0.3;
- Thermal conductivity: 2.0×10^{-2} W/mm-K;
- Coefficient of thermal expansion: 17.37 µm/m-K.

The cylinder deformation is shown in Figure 12. Again the displacement, a maximum of 0.97 mm, occurs mostly along the cylinder axis and is relatively unimportant. The stress plot indicates a stress of 81 MPa along the outside edge of the upper wall curvature toward the connecting duct flange. Other local maximums of 86 MPa are shown at the lower outside radius and inside wall. Because these stresses are lower than the stresses in the regenerator housing, the life limit on the heater head assembly will be limited by the results discussed above for the regenerator housing.

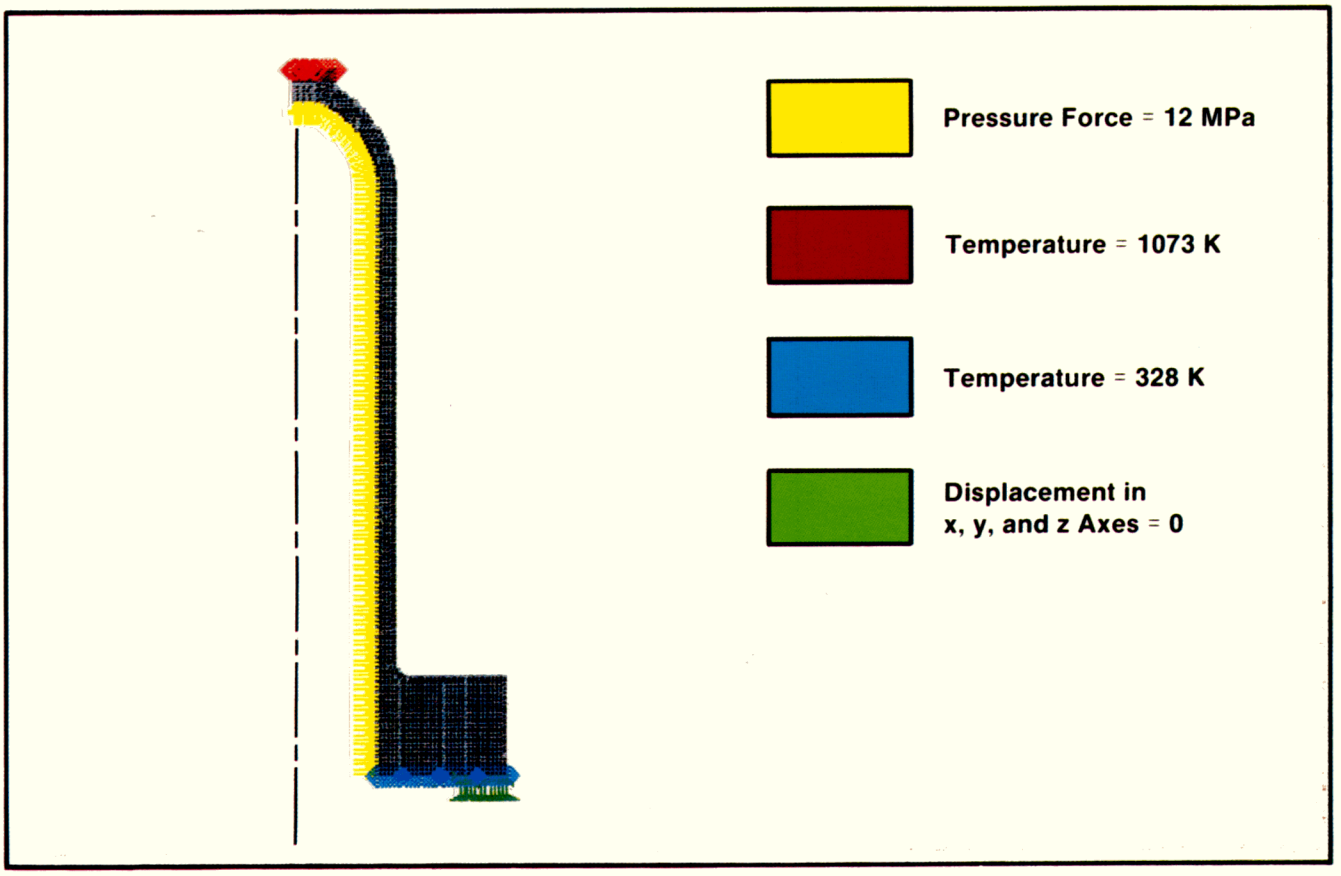

Figure 11. Cylinder element and boundary conditions.

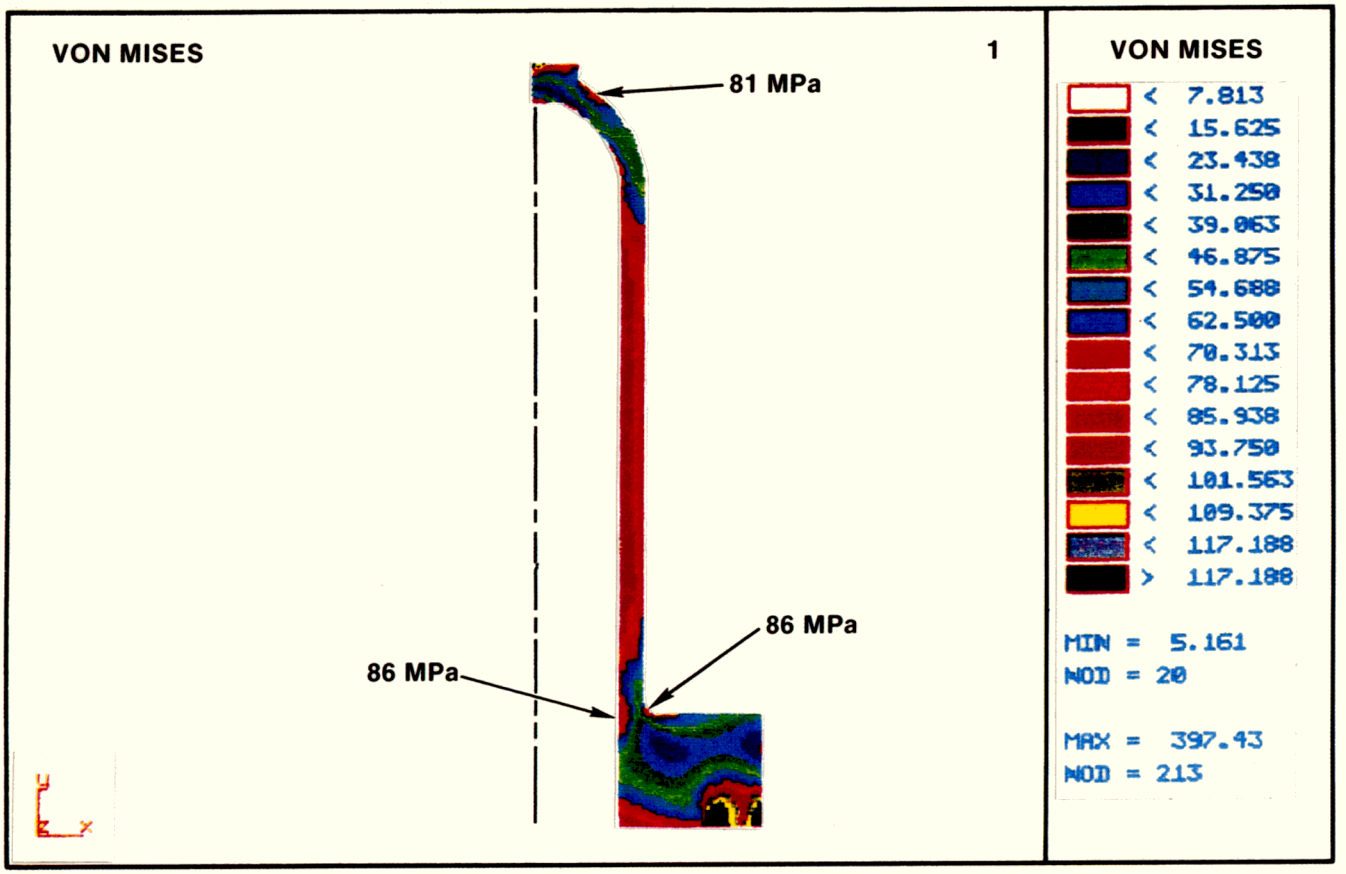

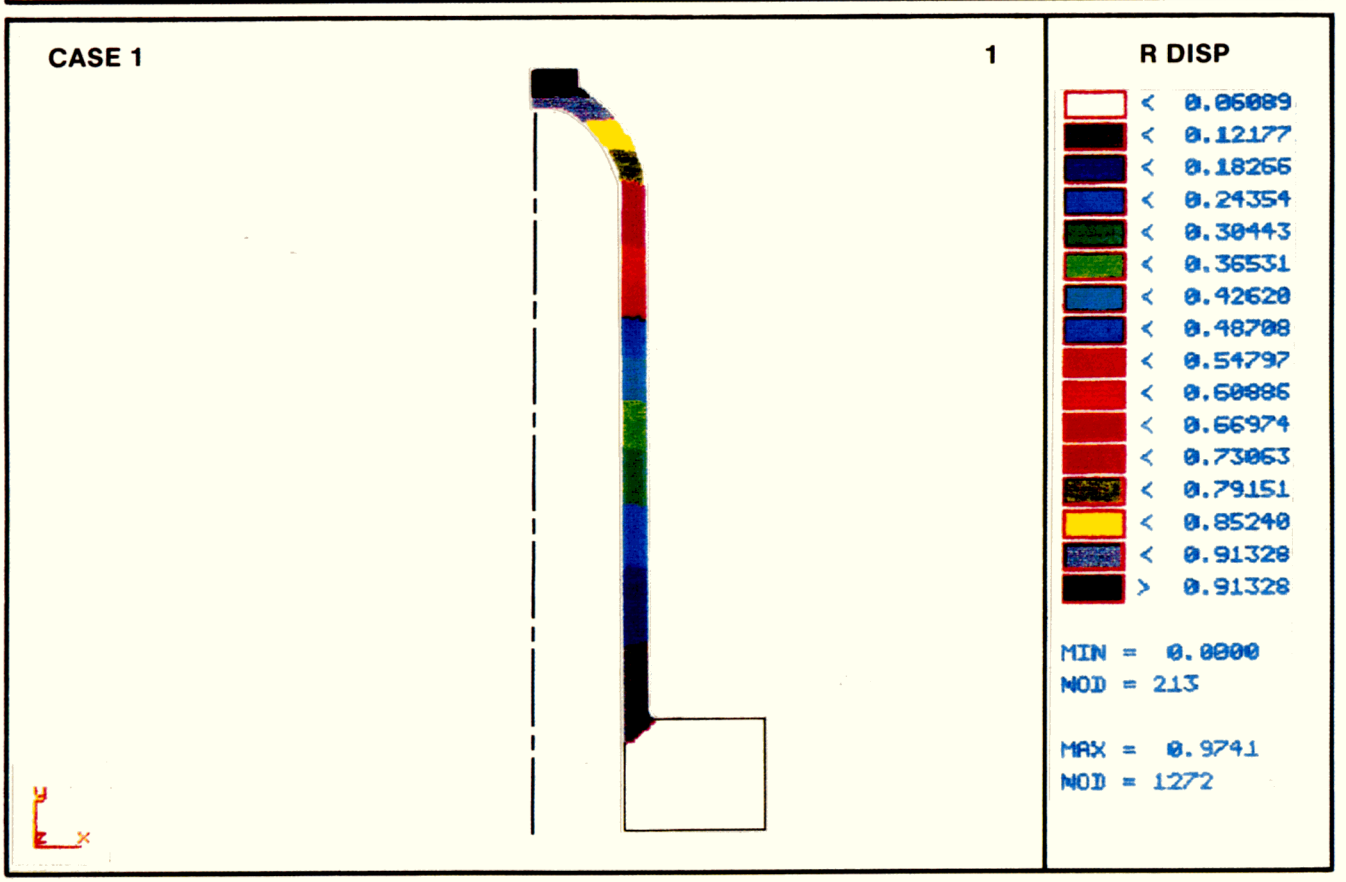

Figure 12. Cylinder stress and displacement.

Pressure Hull

The pressure hull maintains the helium pressure on the crankcase side of the engine. An element and boundary condition plot is shown in Figure 13. With a mean cycle of pressure of 12 MPa, the contained energy in the pressure hull is at 87 kJ; therefore, the component is a pressure vessel and must be designed to meet ASME and SNL pressure-safety standards. These standards require a safety factor of 4.0 based on the ultimate strength of the material. The material used is 4140 steel, a good material choice because it can be heat-treated for additional strength while remaining ductile, an important feature for pressure vessels. The pressure hull is heat-treated to a Rockwell "C" hardness in the 22-29 range. This will result in an ultimate strength between 810 and 900 MPa, with an elongation between 22.5 and 18%, respectively. To maintain a 4.0 safety factor, the stresses should remain under 202 MPa.

The pressure hull was modeled using the following parameters:

- Element type: 4-node quadrilateral, "PLANE2D", axisymmetric;
- Average element size: 2.5 mm;
- Pressure force boundary conditions: 12 MPa applied to all interior element faces (yellow area);
- Temperature boundary conditions: None;
- Displacement boundary conditions: Zero displacement in x and y directions at centerline of bolthole pattern (130 mm from axis), and zero y-displacement radially outward from this point (green area);
- Modulus of elasticity: 2.0×10^5 N/mm^2;
- Poisson's ratio: 0.3.

Figure 14 shows the stress levels and resultant displacements. The displacements are small (0.05 mm) and are of no great concern, except for the radial displacement at the end seal location. STM originally desired a maximum radial displacement of 0.015 mm to prevent O-ring extrusion. Since then, an extrusion ring was incorporated, and the requirement is 0.15 mm. Because the actual displacement is 0.05 mm, this is not an issue. The stresses in the cylindrical hull are more than 250 MPa, so the 4.0 safety factor is not met. To meet the safety factor, the pressure hull wall thickness was increased from 5.0 mm to 6.5 mm and the model was run with the new geometry. The stresses decreased to below 202 MPa, except at the outer edge of the flange (Figure 15). As with the regenerator housing results, these stresses are confined to small areas near the severe boundary conditions and are believed not to be a problem. Future pressure hulls will include this design change so that pressure safety codes are followed. Though the older pressure hulls did not meet the safety factor, all units passed an ASME standard pressure test of 1.5 times the maximum allowable working pressure.

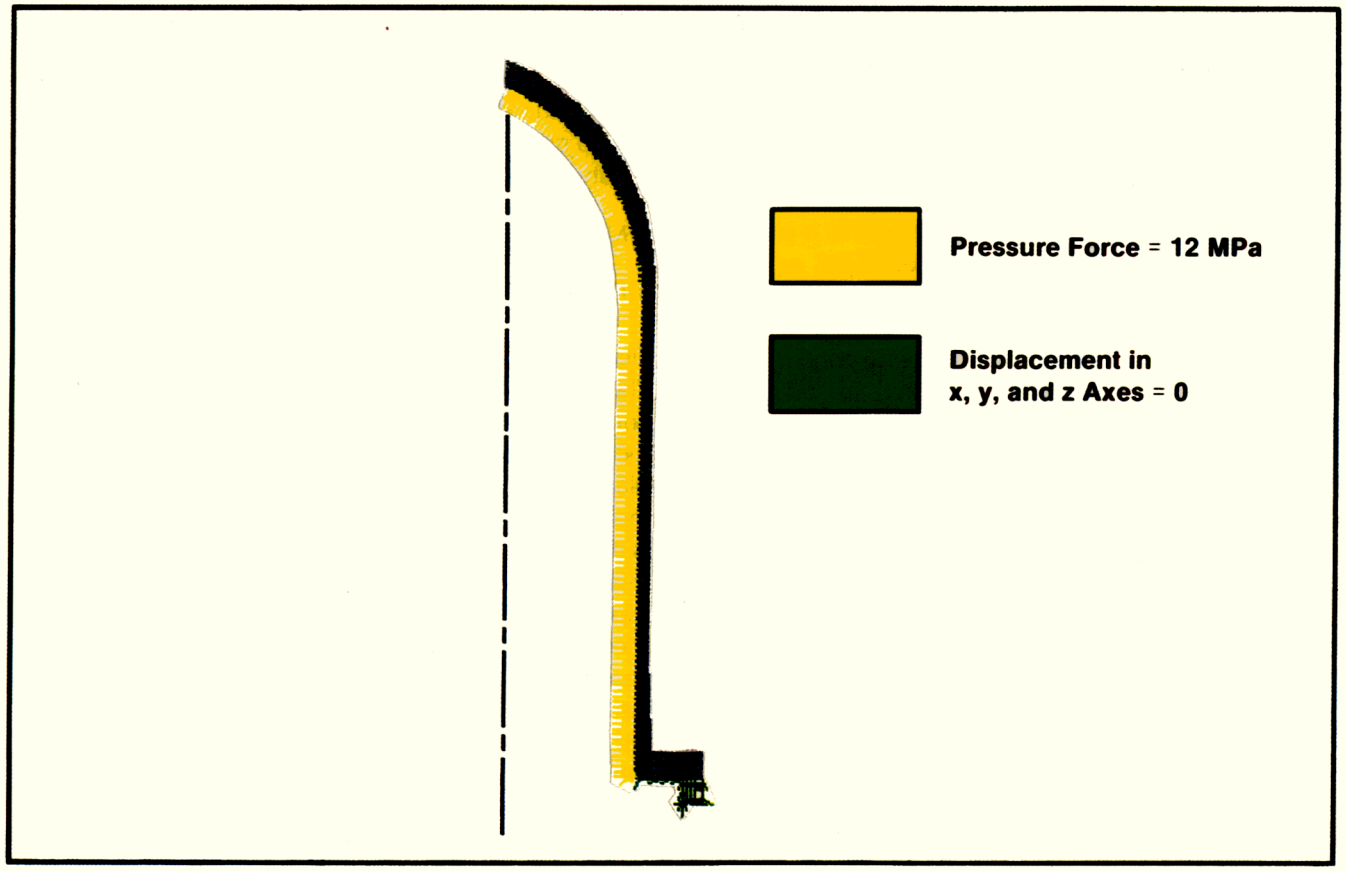

Figure 13. Pressure hull element and boundary conditions.

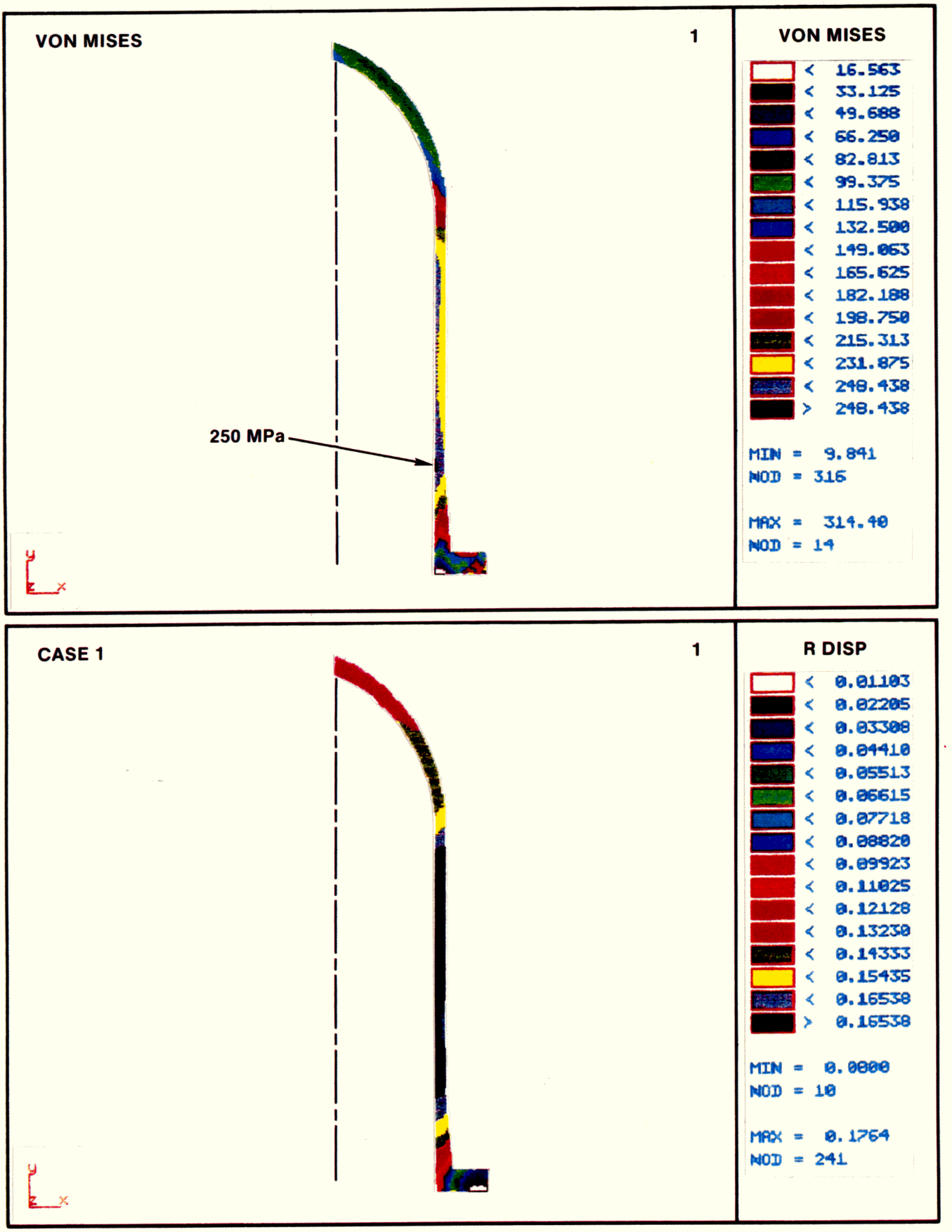

Figure 14. Pressure hull stress and displacement.

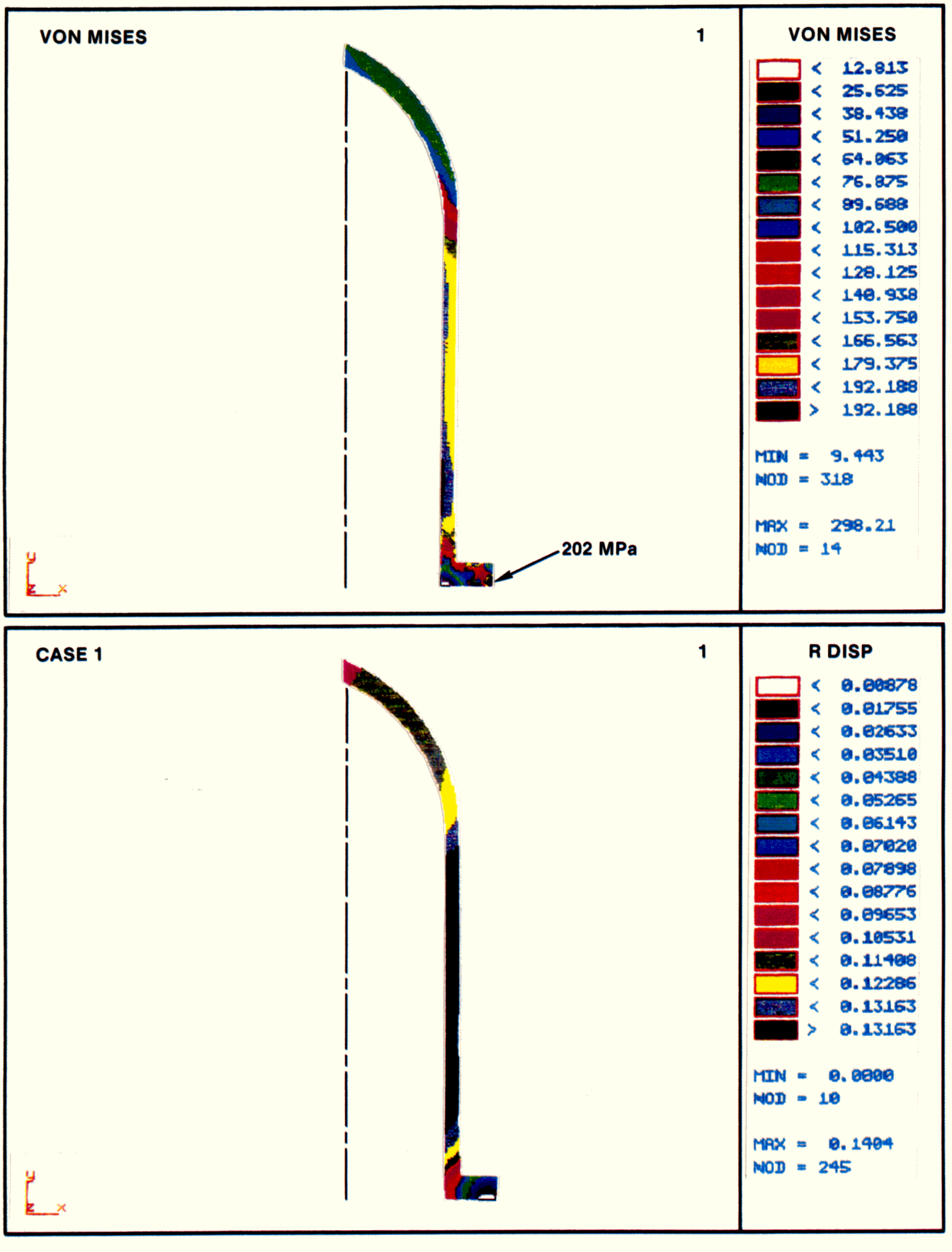

Figure 15. Modified pressure hull stress and displacement.

Oil Sump

The oil sump is located beneath the pressure hull. The oil sump is a pressure vessel that provides a drain point for the oil and contains the oil filter. The element and boundary condition plot is displayed in Figure 16. All the pressure safety requirements described above for the pressure hull apply to the oil sump. The oil sump was modeled using the following parameters:

- Element type: 4-node quadrilateral, "PLANE2D", axisymmetric;
- Average element size: 0.75 mm;
- Pressure force boundary conditions: 12 MPa applied to all interior element faces (yellow area);
- Temperature boundary conditions: None;
- Displacement boundary conditions: Zero displacement in x and y directions at centerline of bolthole pattern (42 mm from axis), and zero y-displacement radially outward from this point (green area);
- Modulus of elasticity: 2.0×10^5 N/mm^2;
- Poisson's ratio: 0.3.

The results of the analysis show that the displacements are small (0.07 mm) and relatively unimportant (Figure 17). Because STM designed the oil sump by scaling down the pressure hull, the stresses in the oil sump are similar. The stresses in the cylindrical hull section are approximately 250 MPa, again violating the 4.0 safety factor. The oil sump was redesigned to meet the safety factor by increasing the wall thickness from 2.0 to 2.6 mm. The results using the new model show the displacements are slight and are acceptable (Figure 18). The stresses dropped below 200 MPa, except for the outer edge of the flange. Once again, these stresses are confined to small areas near the severe boundary conditions and are not of concern. Future oil sumps will include this design change. As with the pressure hulls, all oil sumps are subjected to pressure tests.

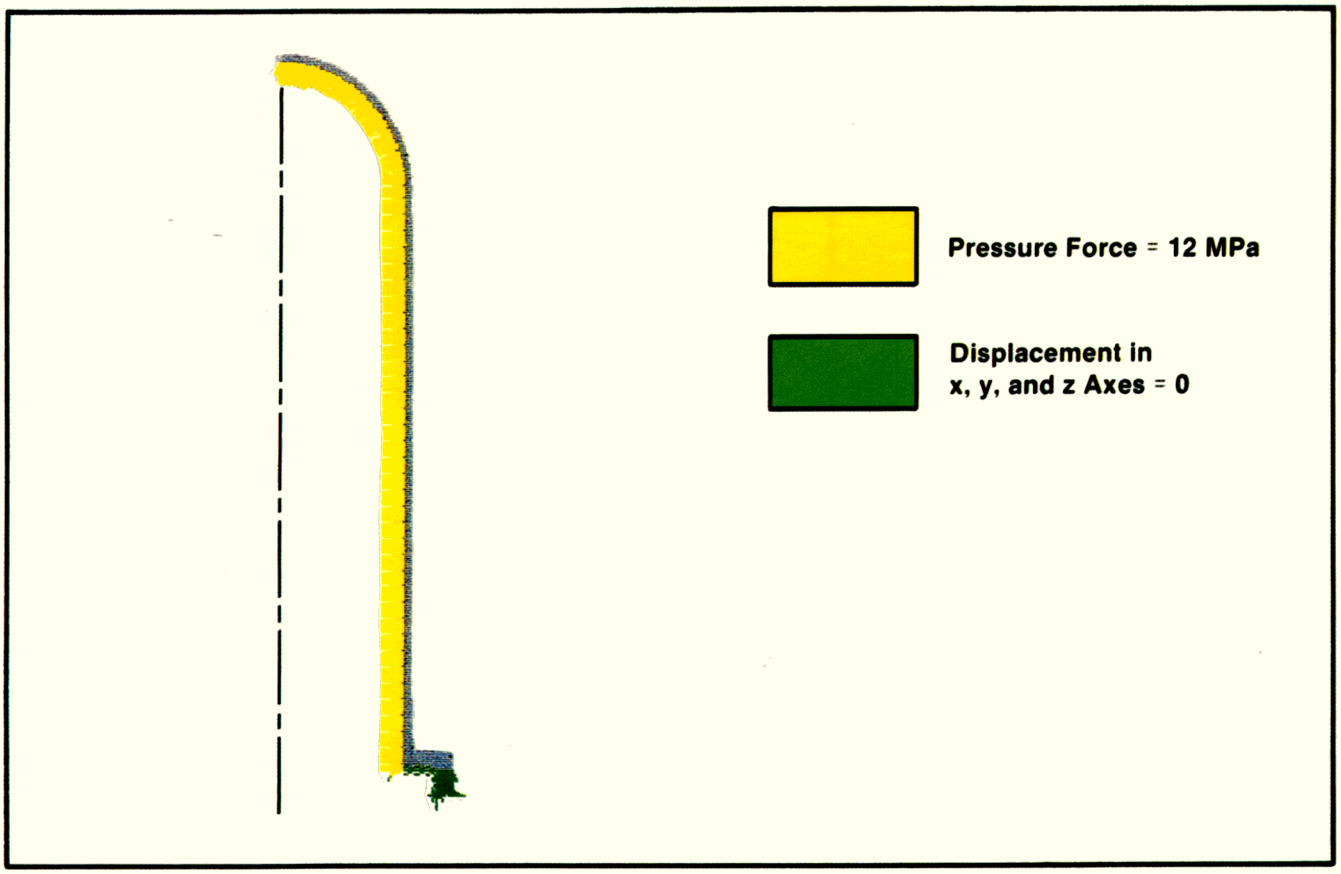

Figure 16. Oil sump element and boundary conditions.

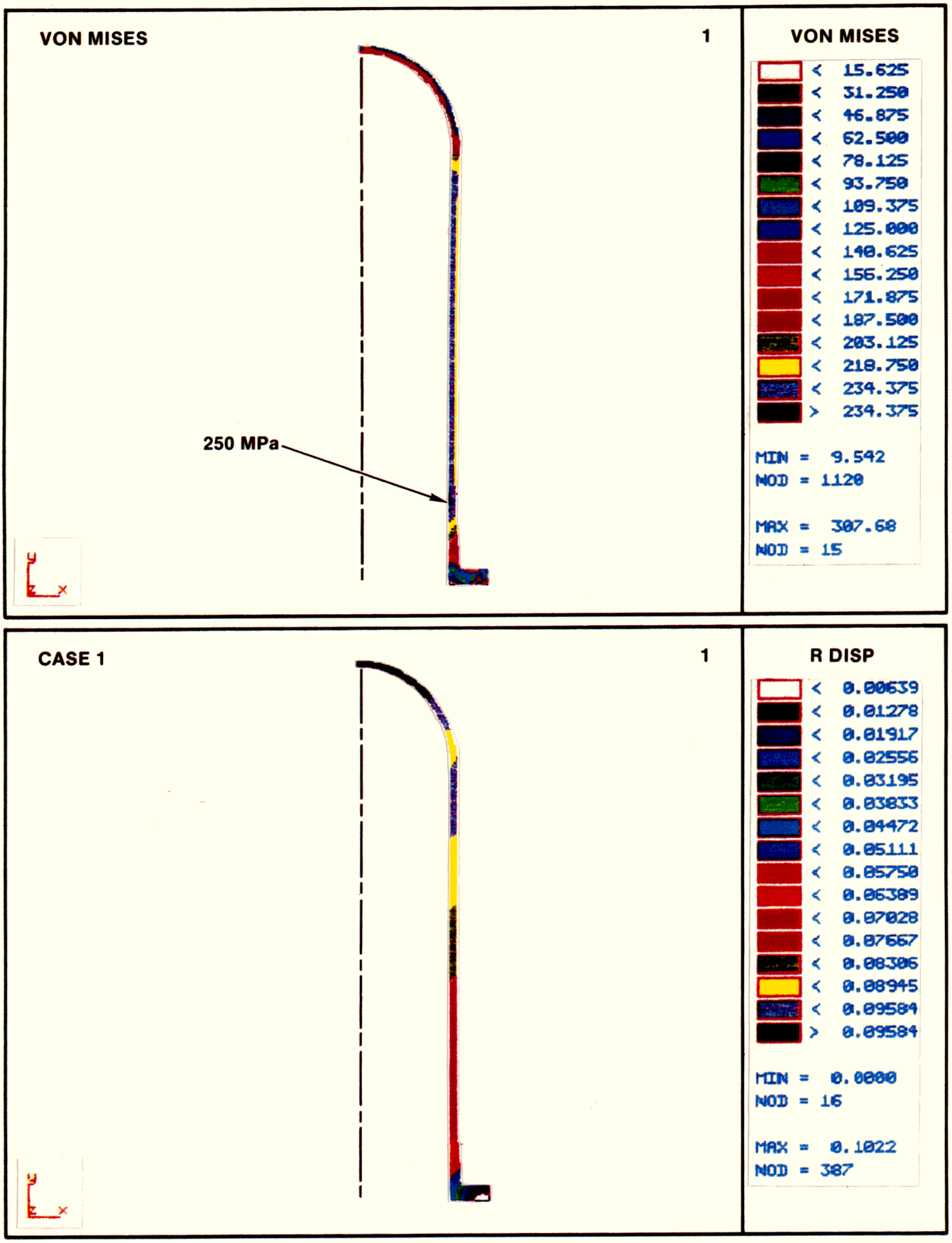

Figure 17. Oil sump stress and displacement.

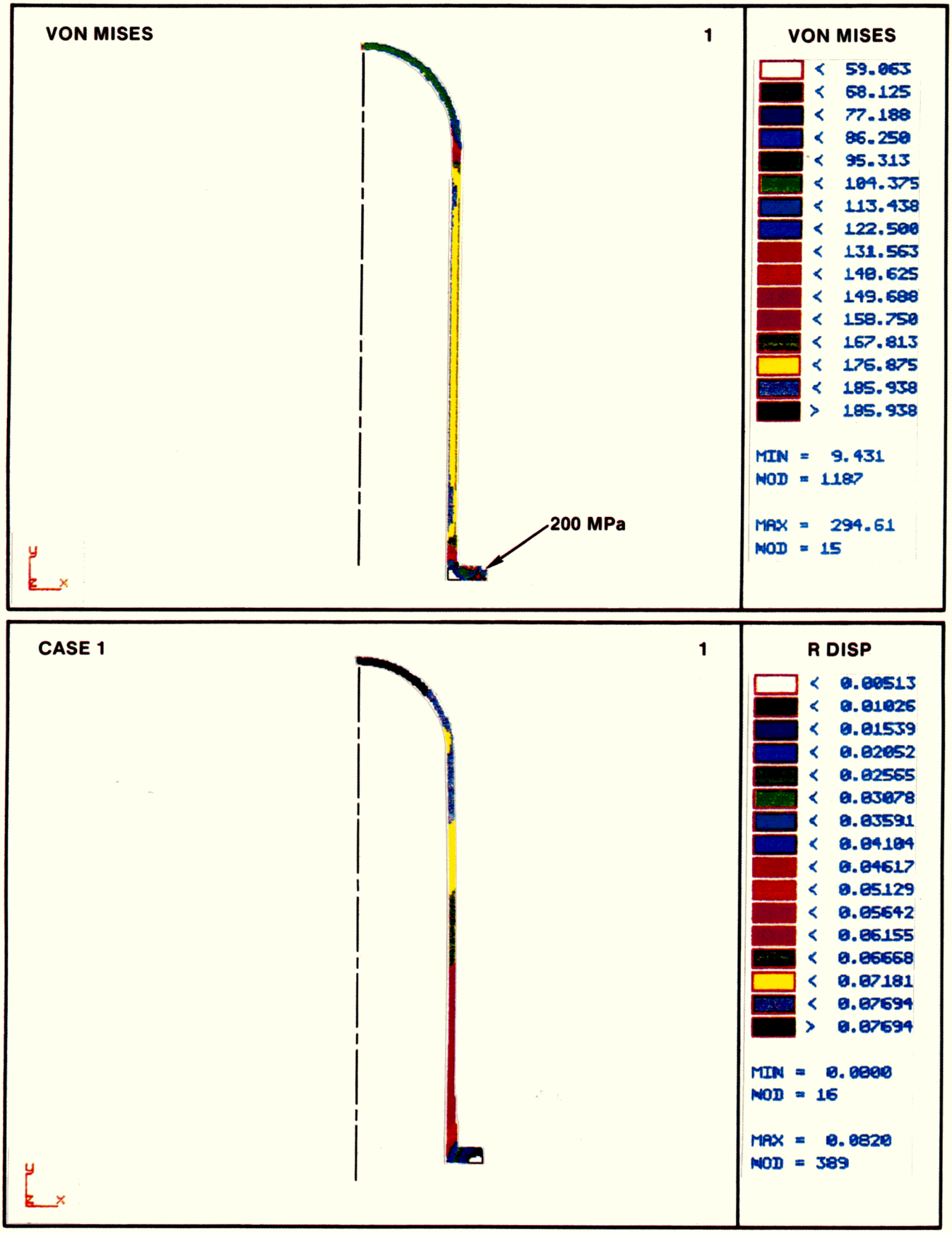

Figure 18. Modified oil sump stress and displacement.

Swashplate

The swashplate is the mechanical device that converts the reciprocating piston motion to rotational shaft power. An FEA (Figure 19) was performed by the authors on this component because concerns had been raised, within SNL, about swashplate mechanisms being highly stressed. The actual swashplate hub axis has a 12.5-degree offset with respect to the swashplate slider-surface axis. For modeling simplicity, these axes are coincident. This approximation is considered valid because the high stresses are in the slider surface, whereas the hub area has very low stresses. This assumption was verified by an FEA using a two-dimensional model.

The swashplate was modeled in three dimensions (Figure 19) using the following parameters:

- Element type: 8-node solid, "SOLID";
- Average element size: 4.5 mm @ 15° intervals about y axis;
- Pressure force boundary conditions: Proprietary, but modeling at maximum loading conditions; color not shown;
- Temperature boundary conditions: None;
- Displacement boundary conditions: No radial displacement on inner hub surfaces parallel to axis of rotation, no y-displacement on surfaces perpendicular to axis of rotation, no radial or y-displacement in threaded nut area (red area);
- Modulus of elasticity: 2.07×10^5 N/mm^2;
- Poisson's ratio: 0.3.

The largest displacement is at the edge of the swashplate ring and is quite small (0.05 mm) (Figure 20). The stresses are under 100 MPa. (This ignores the peak stress of 101 MPa at the point force application. Actually, the force is distributed over a larger area through the crosshead slider, which would reduce this peak stress.) The highest stresses are located where the slider surface meets the outer hub surface. This is reasonable because the piston forces are on a plate cantilevered from the hub area (the highest stresses on a cantilever beam occur at the fixed end of the beam). Stresses are low in the hub area, so the approximation of the hub and slider axes being coincident is reasonable. It is interesting to note that the two-dimensional model predicted results very similar to those for a three-dimensional model. Finally, because the stresses are well under the endurance limit for the material used (8620 steel, carburized to a Rockwell "C" surface hardness in the 58-62 range), fatigue problems are not expected.

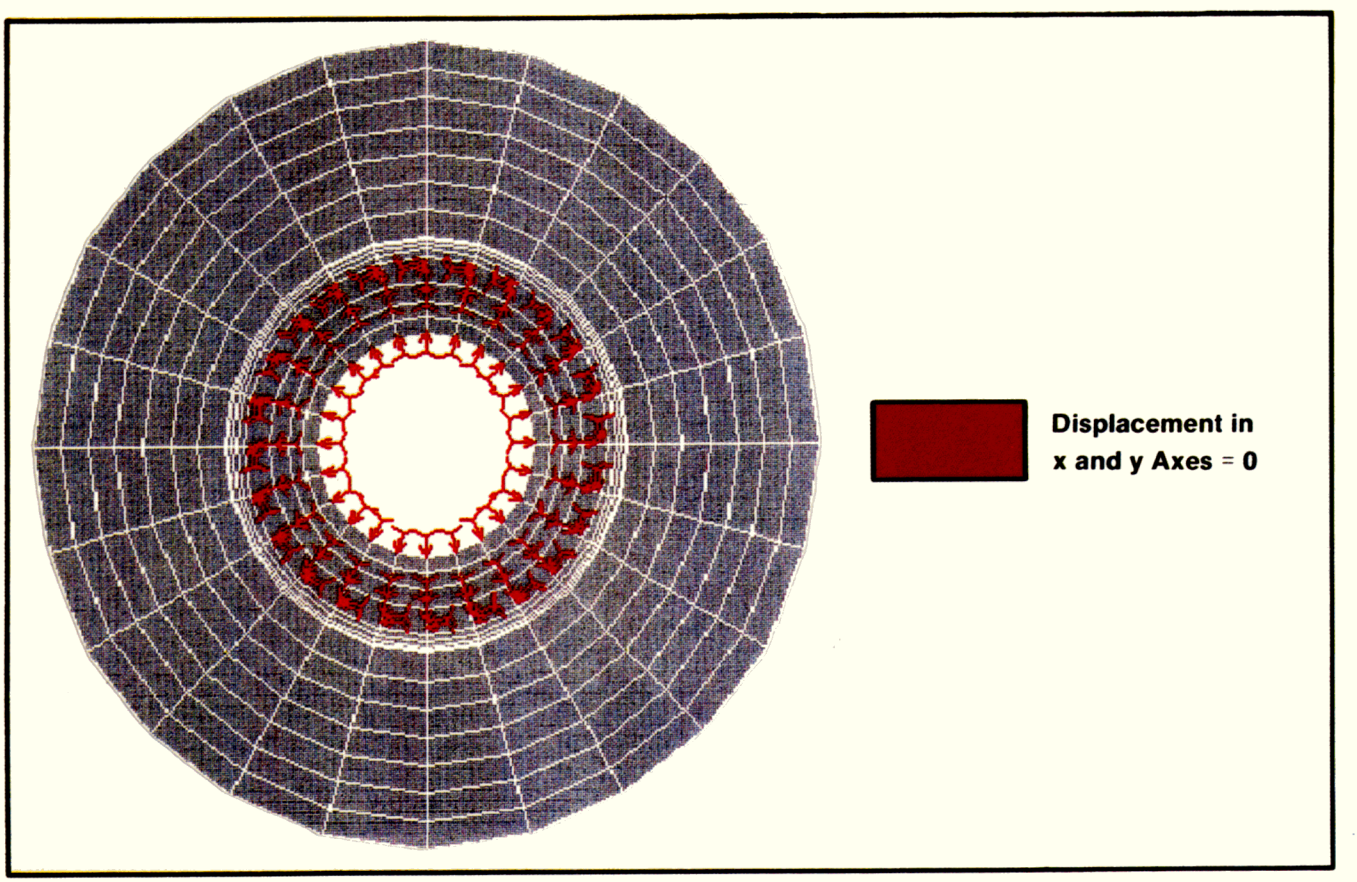

Figure 19. Swashplate element and boundary conditions.

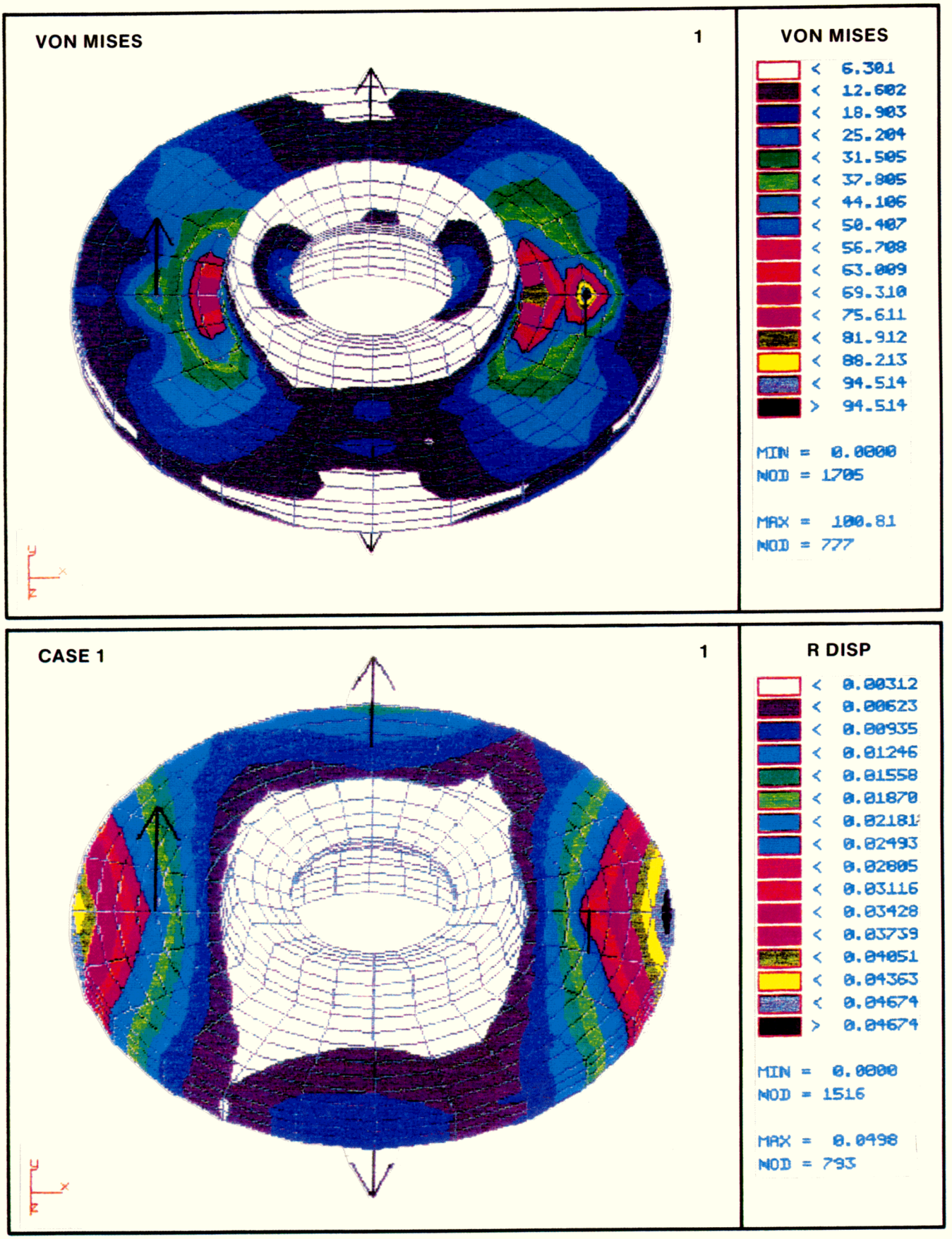

Figure 20. Swashplate stress and displacement.

IV. SCOPE OF TESTING

The testing will establish the overall performance of the Stirling Thermal Motors, STM4-120 kinematic Stirling engine for solar thermal applications. The performance includes not only the power and efficiency, but also the reliability of the engine. In the past, the issue of reliability of Stirling engines has been a major concern. The STM4-120 has been designed to address reliability issues that have plagued other Stirling engines.

The test parameters will be characterized for various operating conditions such as heater head temperature, cooling fluid temperature, piston stroke, and working gas pressure. Planned operations for performance mapping are shown as a matrix (Figure 21). These operations include documenting the cause of a problem along with the time and material required to correct the problem, which will help to establish a data base for free operation and maintenance of Stirling engines and, in particular, the STM4-120 Stirling engine. The Appendix of this report gives a detailed list of the problems encountered during the initial testing.

The STM4-120 is presently installed in a test cell at Sandia's ETF. Gas-fired combustors provide heat to the sodium heat pipes, which then drive the engine. Shaft power output from the engine is absorbed by an eddy-current dynamometer.

Engine Test System Layout and Instrumentation

The STM engine test system consists of the dynamometer, the engine/dynamometer skid, the dynamometer cooling system, the engine cooling skid, the combustion skid, the helium supply system, the instrumentation with the associated data acquisition system (DAS), and the emergency control unit (ECU) (Figure 22). Each of these systems is discussed in the following sections.

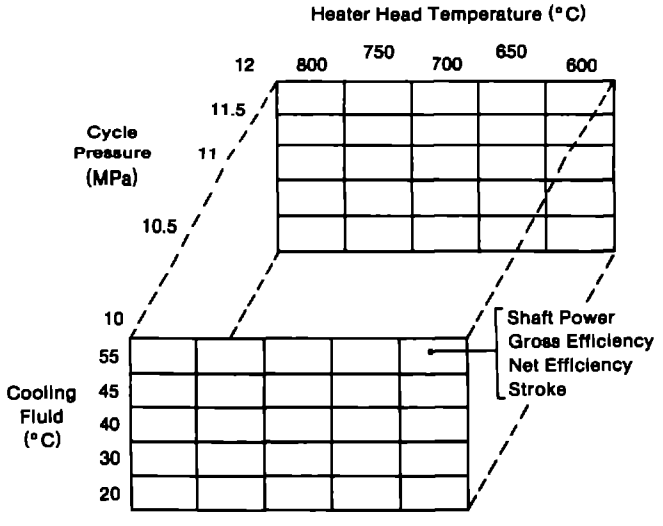

Figure 21. Test matrix.

DYNAMOMETER

An eddy-current dynamometer is used in the test. Electrical current flowing through the excitation coil induces a magnetic field. A toothed rotor rotating through the field produces eddy currents that build up a magnetic field that opposes the torque produced by the engine. The mechanical energy from the engine is converted into heat via the eddy currents, and the heat is removed by the dynamometer cooling water.

The dynamometer can be operated in either a torque control mode or a speed control mode. In torque control mode, a constant opposing torque is applied to the motor under test and the speed may vary. In speed-control mode, the dynamometer control unit adjusts the opposing torque to maintain a desired speed. The STM engine test uses the speed control mode with a setpoint of 1800 rpm.

ENGINE/DYNAMOMETER SKID AND INTERFACE

The engine/dynamometer skid is a test stand for the engine, the dynamometer, and the four gas-fired heat pipes (Figure 23). The skid is fabricated from I-beam and C-channel and is a rigid structure. Vibration pads isolate the skid from the concrete floor.

To avoid errors in measuring the engine's performance, the engine and dynamometer axes must be kept aligned. To accomplish this alignment, the following procedure was performed. The dynamometer was bolted to the test stand base. Then the engine was placed on, and loosely bolted to, the engine stand. The engine was positioned and shimmed until the engine and dynamometer shafts were aligned with respect to parallelism (0.003-in. vertical plane and 0.006-in. horizontal plane) and center-to-center location (0.010-in. vertical plane and 0.014-in. horizontal plane). This engine location was then attached to the engine bracket/stand interface and stand/base interface. Tapered pins were used through the engine brackets to allow for removal and subsequent reinstallation of the engine while maintaining the engine/dynamometer alignment.

Before engine startup, the engine is "motored," or rotated at 740 rpm at a piston stroke of 5 mm. This minimizes the temperature gradient through the cycle side of the engine as the heater heads are brought up to temperature, thus reducing thermal stresses. The dynamometer used does not have this motoring capability, so an electric motor and

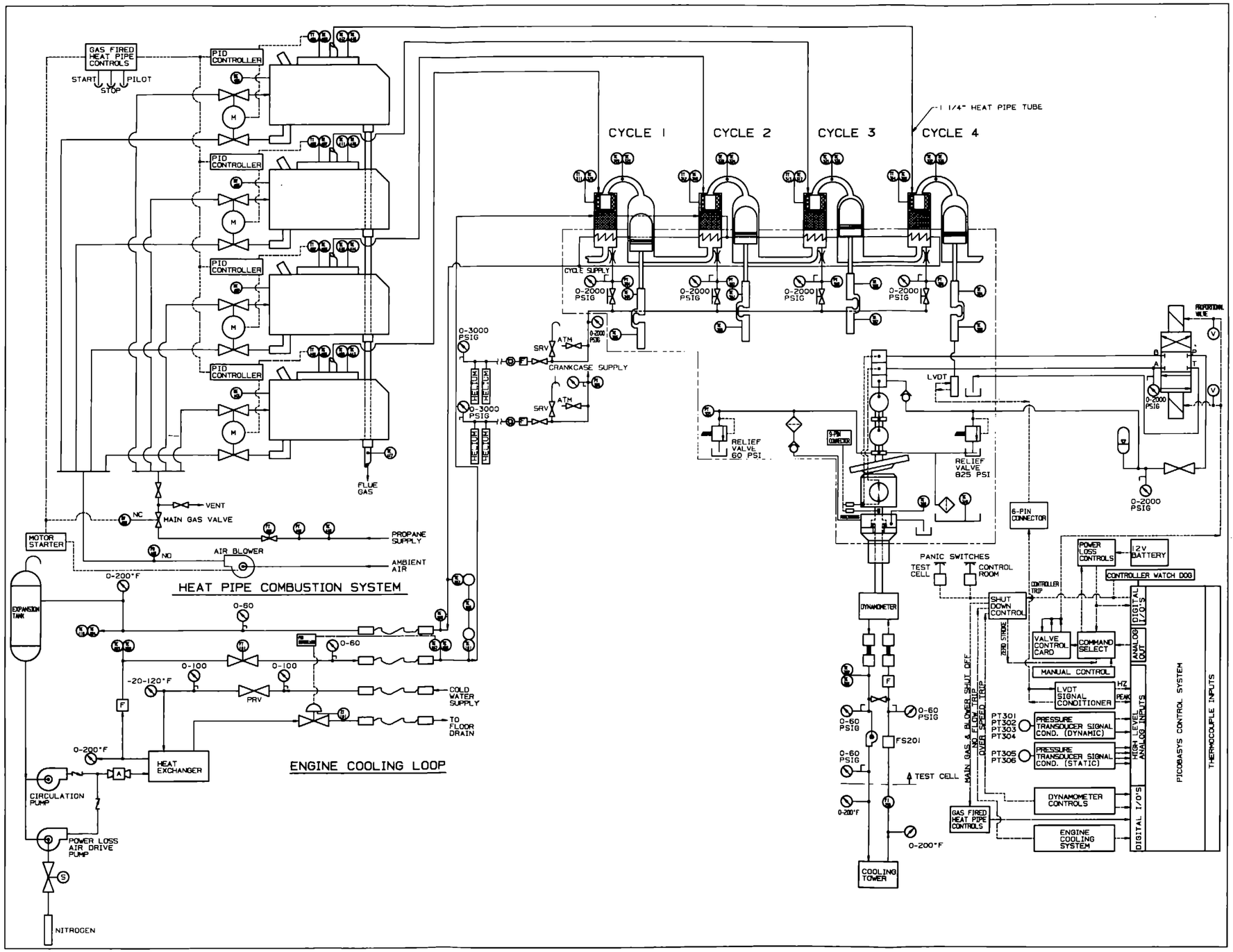

Figure 22. Schematic diagram of STM4-120 test.

pulley system are used. A square tube frame was fabricated and welded to the test stand base (Figure 23). A hinged platform was attached to the frame that extends above the centerline of the dynamometer, and a 5-hp electric motor was mounted to the platform. A commercial sheave was modified and placed between the dynamometer shaft and the driveshaft. When the engine needs to be motored, an air cylinder drives the platform upward, tensioning the belt between the electric motor and the dynamometer shaft, which rotates the output shaft of the engine.

The test stand also holds the exhaust manifold for the combustors, supports the exhaust hose, and provides a mounting point for the hydraulic swashplate control valve and for a terminal strip enclosure.

DYNAMOMETER COOLING SYSTEM

The energy absorbed by the dynamometer is converted to heat that is removed from the system. The dynamometer cooling system consists of a 5-hp centrifugal pump, a dry-type cooling tower (outside the test cell), a magnetic filter (designed to protect the dynamometer), and associated piping and valving. An air separator and an expansion tank eliminate water "hammer."

The cooling tower contains three fans. One fan is powered as soon as the breaker is closed. The other two fans are controlled with thermostats and start only if the temperature rise is sufficient to require the extra cooling.

The coolant used is a 50/50 mixture of water/glycol at a flow rate of 57 l/min. The flow rate can be visually verified with a flowmeter. The system also contains a flow switch connected to both the hardware safety system and to the control system. The engine cannot be operated if the flow switch is not activated.

ENGINE COOLING SKID

The engine cooling skid provides an accurate method of controlling the cooling water inlet temperature. A 50/50 water/glycol mixture is circulated at a flow rate of 159 l/min. The coolant is first pumped through an automatic flow controller, a tube and shell heat exchanger, a filter, and a turbine flowmeter, and then through the engine and back to a vented surge tank. The inlet temperature is maintained by controlling the flow rate of raw water through the shell side of the heat exchanger. The coolant temperature is transmitted to a piping and instrumental diagram (PID) controller via a cooling water inlet

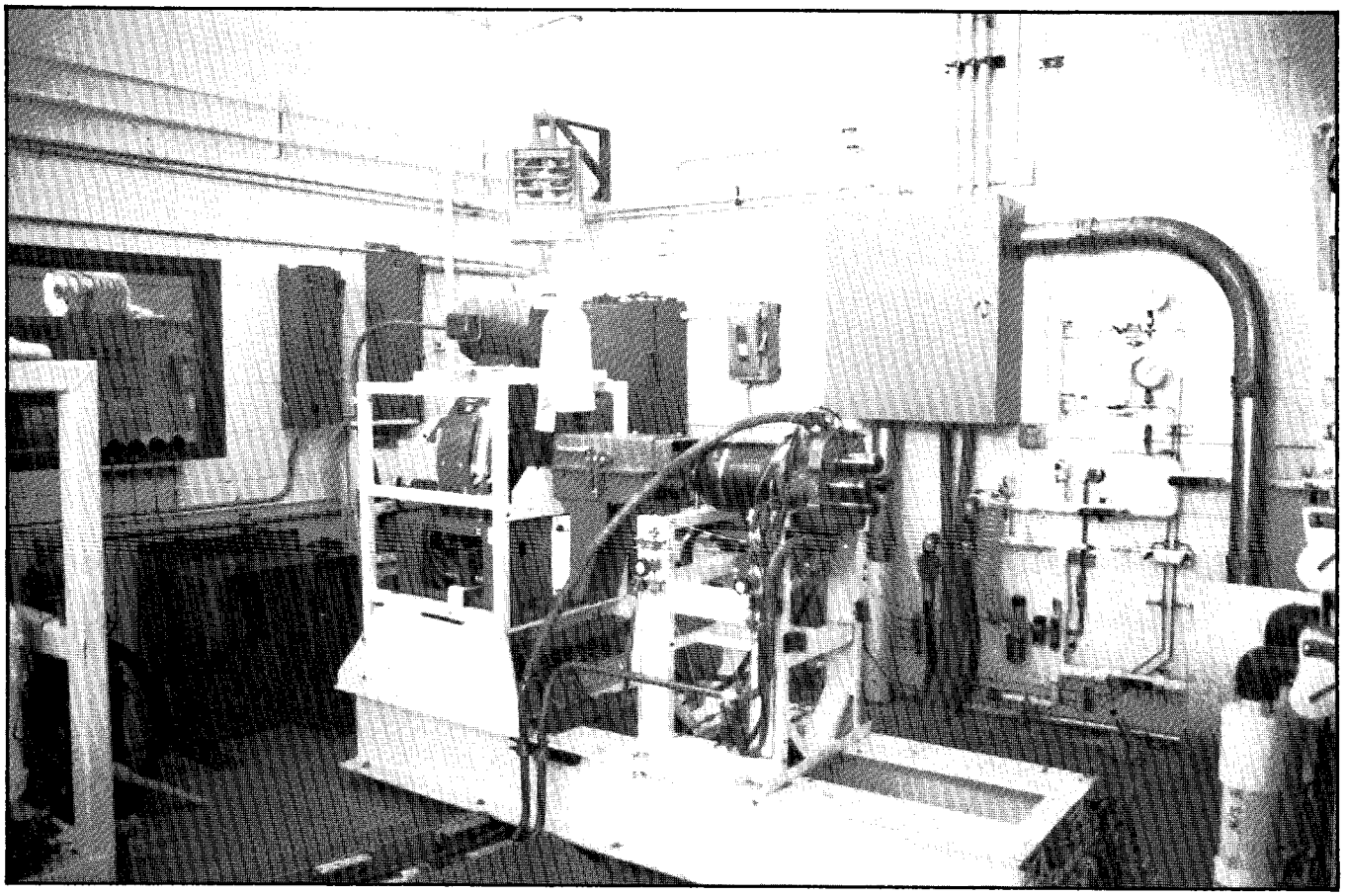

Figure 23. Test stand.

thermocouple. Based on the setpoint temperature, the PID controller sends the appropriate current signal to the actuator on the control valve, adjusting the raw water flow rate to maintain the setpoint. Although the system may appear elaborate for removing 30 kW of heat, the complexity is required to control the coolant temperature accurately when mapping the engine performance.

During prototype testing, maintaining coolant flow is important even after the engine is shut down. This is a precautionary measure to avoid any thermal stress in the engine cylinder block. To ensure cooling during a power outage, an air-driven motor and small pump were placed in parallel with the main pump. In the event of a power outage, a normally open solenoid valve on the air supply opens, activating the small pump and circulating approximately 19 l/min of coolant through the engine.

COMBUSTION SKID

The combustion skid contains the system to deliver and control the fuel/air flows to the four combustors, thereby controlling the heat pipe evaporator temperatures. The evaporator thermocouple signals are transmitted to the PID controllers, which output a current signal to the valve controllers that are mechanically linked to the air and fuel valves. The valves are micro-ratio valves, in which the port opening is determined by the shape of a cam on which the valve rides. The shape of the cam is adjustable by hex-head screws that deform the cam. The air and fuel valves are initially adjusted to provide the desired mass flow rates throughout the valve travel.

The combustion skid also consists of the piping and electronics to ignite, deliver, and safely control the propane. The propane inlet piping contains a "block and bleed" system to contain the gas. This system consists of a main gas valve, a vent valve, and a blocking valve. There are two valves in series to prevent propane flow except during operation. Also, the skid contains the flame sensor electronics to monitor the ultraviolet (UV) sensors mounted on the combustion chambers. If a flame is not detected in any of the combustors, the main gas valve and blocking valve are automatically closed so that unburned propane is not collected in the combustors or the exhaust system.

HELIUM SUPPLY

Helium is supplied to both the gas-cycle side and crankcase side of the engine. The two sources are completely independent, eliminating the possibility of contaminating the gas cycle side of the engine with crankcase oil. The helium bottles and manifolds, located outside the test cell, connect to 1/4-in. stainless steel tubing running into the test cell. Each supply line contains a pressure regulator, a filter, shutoff and vent valves, a safety relief valve, and pressure gages. The lines are then routed to the engine. The cycle supply line branches off into four individual cycle lines. Each cycle line contains a shutoff valve near the engine to reduce the dead space volume. Due to the difficulty in containing helium, nearly all of the plumbing connections are silver-soldered. After low power tests were completed, the pressure regulators were moved inside the control room to eliminate the need for a person to enter the test cell to change the mean cycle pressure.

INSTRUMENTATION

Because the STM engine is being fully tested for the first time, the engine and heat pipes have been completely instrumented. The instrumentation includes thermocouples, pressure transducers, volumetric and mass flowmeters, UV sensors, dynamometer output signals, signal transmitters, and controllers. The transducer types and general instrumentation practices are discussed below.

Temperature

The engine contains sheathed type-K thermocouples for the front and rear crossheads, oil sump, and end seal. The heat pipes include dual sheathed thermocouples (1/16 in.) for the individual temperatures of the heater heads, connecting ducts, and front and rear evaporators. Dual thermocouples (one thermocouple signal was transmitted to the DAS and the other to the ECU) were used where possible for redundancy and to avoid paralleling a single thermocouple to several data analysis or recording devices. All the thermocouples in the heat pipes are placed in thermowells to obtain an accurate vapor temperature while allowing easy replacement.

The engine cooling system instrumentation contains mostly type-T thermocouples (which are more accurate than type-K thermocouples) for cooling water inlet and outlet temperatures. The dynamometer cooling system contains mechanical temperature gages plus type-K thermocouples for the dynamometer water outlet temperature. Finally, a type-T thermocouple is used to measure propane temperature.

Accuracies of type-K thermocouples are ±2.8°C in the 0° to 349°C range, and ±0.75% in the 350° to 1260°C range. Accuracies of type-T thermocouples are ±0.5% or ±0.8°C (whichever is greater) in the -59° to 93°C range, and ±0.75% in the 94° to 371°C range [15].

Pressure

In addition to mechanical pressure gages, helium cycle pressure and crankcase pressure are measured with full-bridge pressure transmitters. These transmitters are accurate

(±0.25% of span) and are much more stable than the half-bridge pressure transducers previously used.

Other pressure measurements include mechanical pressure gages for the dynamometer cooling loop and two pressure transmitters for the propane. These transducers have a stated accuracy of 0.25% of calibrated span. Stability is 0.25% of upper range limit for six months, and the effect of temperature is 0.2% of range plus 0.2% of span per 20°C.

Flow Rate

To calculate engine and system efficiencies, the mass flow rate of propane is needed. Originally, mass flow rate was calculated by measuring the total volumetric flow rate along with the propane temperature and pressure. To obtain more accurate measurements and to be able to tune and trouble-shoot each heat pipe, mass flowmeters were plumbed into the propane and air lines leading to each of the four combustion chambers. These flowmeters contain a hot probe maintained at a constant temperature. The current required to maintain the constant temperature is proportional to the mass flow rate. The accuracy of the flowmeters, according to the manufacturer's published specifications, is ±2% plus 1/2% of full scale.

As mentioned above, a turbine flowmeter is used to measure the total propane flow (with temperature and pressure) as a comparison to the sum of the four mass flow rates. Turbine meters are also used to measure the volumetric flow of the engine cooling water. The magnetic pulses from the turbine flowmeters are run into a pulse rate converter, which measures the number of pulses in a given time frame and converts the signal to a 4-to-20-mA current output. Accuracies of the turbine flowmeters, per the manufacturer, are about ±2%.

UV Sensors

As mentioned earlier, the UV sensors are mounted on a pipe inserted into each combustion chamber. The UV sensors respond to any UV, so it is important that the sensor "see" only the flame and no other UV sources. Before and during start up, the UV sensors are shunted from the system. This avoids false signals and erroneous shut downs. After start up, a loss of the current signal generated by the UV sensor would open a relay in the safeguard. The combustion skid is wired so that a flameout on any of the four burners will immediately close the propane main gas valve and blocking valve.

Engine Torque and Speed

Engine torque and speed signals are sent to the dynamometer controller in the control room through dedicated cables. Engine torque is determined by the force applied to a load cell located between the dynamometer casing and the fixed base. Because the distance from the centerline of the dynamometer to the load cell is known, the torque is computed by multiplying the force by the known distance, while the power is computed from the torque and speed. Engine speed is measured by a magnetic pulse and counter system internal to the dynamometer casing. The torque and speed signals are digitally displayed on the control unit and are also output from the back panel on the control unit to the data acquisition system.

The system is calibrated by mounting lever arms on either side of the dynamometer casing. Calibrated weights are placed in the lever arm weight trays. Potentiometers are then adjusted to match the measured signal with the known torque. The accuracy of the torque signal is ±0.4% of the dynamometer's maximum torque loading of 400 N-m, so the torque accuracy is ±1.6 N-m. The accuracy of the speed signal is ±1 rpm.

General Information

Some of the TCs are run through transmitters to allow for multiple signal destinations and devices that cannot accept a low-level voltage signal. Current transmitters are used whenever possible to eliminate noise problems associated with long line lengths. The instrumentation wiring between these various systems is protected by conduit mounted to the walls. All instrumentation wiring terminates inside a junction box inside the test cell. The wires are routed outside through a vented pull box, then back underneath the test cell into terminal strips inside the control room. The signals are then transmitted to the various devices such as the data system, the emergency control unit, panel meters, stripcharts, indicating lamps, and controllers.

DATA ACQUISITION SYSTEM

The data acquisition system (DAS) measures, displays, and stores the data from each data channel in the system. The DAS is composed of a personal computer coupled with a scanner/voltmeter. The data measured are displayed on the monitor and stored on a hard disk. The system can scan the 73 channels in 5 seconds (see Table 1). The scanner/voltmeter contains both a slow-speed and a high-speed voltmeter. Initially, the high-speed voltmeter was used for the higher level signals (>0.1 V) and temperatures where the stated ±2°C accuracy is acceptable, while the slow-speed voltmeter was used for more critical thermocouple channels. However, noise problems and ±3°C "jitter" in the high-speed voltmeter mandated using the slow-speed voltmeter, which integrates the signal, eliminating any noise superimposed on the low-level signal. Future enhancements will include a graphical display of the engine and heat pipes containing real-time data.

Table 1. STM4-120 Instrumentation and Controls

SYSTEM: ENGINE PARAMETER	SIGNAL DESTINATION	OPERATING RANGE	SYMBOL	TYPE	EMERGENCY SHUTDOWN LIMIT
FX-HEAD 1	DAS & ECU	0-100°C	TE301	TC, K	>100°C
FX-HEAD 2	DAS & ECU	0-100°C	TE302	TC, K	>100°C
FX-HEAD 3	DAS & ECU	0-100°C	TE303	TC, K	>100°C
FX-HEAD 4	DAS & ECU	0-100°C	TE304	TC, K	>100°C
RX-HEAD 1	DAS & ECU	0-100°C	TE305	TC, K	>100°C
RX-HEAD 2	DAS & ECU	0-100°C	TE306	TC, K	>100°C
RX-HEAD 3	DAS & ECU	0-100°C	TE307	TC, K	>100°C
RX-HEAD 4	DAS & ECU	0-100°C	TE308	TC, K	>100°C
END SEAL	DAS & ECU	0-100°C	TE309	TC, K	>100°C
OIL SUMP	DAS & ECU	0-100°C	TE310	TC, K	>100°C
HEATER HEAD 1	X-MITER TO DAS, STRIP	0-1000°C	TT311	TC, K	
HEATER HEAD 2	X-MITER TO DAS, STRIP	0-1000°C	TT312	TC, K	
HEATER HEAD 3	X-MITER TO DAS, STRIP	0-1000°C	TT313	TC, K	
HEATER HEAD 4	X-MITER TO DAS, STRIP	0-1000°C	TT314	TC, K	
HEATER HEAD 1	ECU	0-1000°C	TE315	TC, K	>810°C
HEATER HEAD 2	ECU	0-1000°C	TE316	TC, K	>810°C
HEATER HEAD 3	ECU	0-1000°C	TE317	TC, K	>810°C
HEATER HEAD 4	ECU	0-1000°C	TE318	TC, K	>810°C
CONNECTING DUCT 1	DAS	0-1000°C	TE319	TC, K	
CONNECTING DUCT 2	DAS	0-1000°C	TE320	TC, K	
CONNECTING DUCT 3	DAS	0-1000°C	TE321	TC, K	
CONNECTING DUCT 4	DAS	0-1000°C	TE322	TC, K	
CONNECTING DUCT 1	ECU	0-1000°C	TE323	TC, K	>810°C
CONNECTING DUCT 2	ECU	0-1000°C	TE324	TC, K	>810°C
CONNECTING DUCT 3	ECU	0-1000°C	TE325	TC, K	>810°C
CONNECTING DUCT 4	ECU	0-1000°C	TE326	TC, K	>810°C
CYCLE 1 PRESSURE	DAS & ECU	0-15 MPa	PT301	PRESSURE TRANSDUCER	>12 MPa
CYCLE 2 PRESSURE	DAS & ECU	15 MPa	PT302	PRESSURE TRANSDUCER	>12 MPa
CYCLE 3 PRESSURE	DAS & ECU	15 MPa	PT303	PRESSURE TRANSDUCER	>12 MPa
CYCLE 4 PRESSURE	DAS & ECU	15 MPa	PT304	PRESSURE TRANSDUCER	>12 MPa
LUBE OIL PRESSURE	DAS & ECU	0-300 psia	PT305	PRESSURE TRANSDUCER	<172 KPa
CRANKCASE PRESSURE	DAS & ECU	0-15 MPa	PT306	PRESSURE TRANSDUCER	>12 MPa
STROKE FEEDBACK	DAS, ECU, STRIP	0-48.5 mm, 0-10V	ZT301	LVDT	
ENGINE SPEED (FROM ENGINE)	DAS & ECU	0-2000 RPM	ZT301	FREQUENCY TRANSDUCER	>2000 RPM
ENGINE SPEED (FROM DYNAMOMETER)	DAS & STRIP	0-2000 RPM		DYNAMOMETER FUNCTION	
ENGINE TORQUE (FROM DYNAMOMETER)	DAS, ECU, STRIP	0-2000 RPM		DYNAMOMETER FUNCTION	>170 N-M
STROKE INPUT	DAS,VALVE CONTROL CARD	0-10V	ZT302	POTENTIOMETER	
FRONT EVAPORATOR TEMPERATURE 1	X-MITER, HPCONTROL, DAS, DPM	0-1000°C	TT401	TC, K	
FRONT EVAPORATOR TEMPERATURE 2	X-MITER, HPCONTROL, DAS, DPM	0-1000°C	TT402	TC, K	
FRONT EVAPORATOR TEMPERATURE 3	X-MITER, HPCONTROL, DAS, DPM	0-1000°C	TT403	TC, K	
FRONT EVAPORATOR TEMPERATURE 4	X-MITER, HPCONTROL, DAS, DPM	0-1000°C	TT404	TC, K	
FRONT EVAPORATOR TEMPERATURE 1	OVER TEMPERATURE CONTROLLER	0-1000°C	TE405	TC, K	>810°C
FRONT EVAPORATOR TEMPERATURE 2	OVER TEMPERATURE CONTROLLER	0-1000°C	TE406	TC, K	>810°C
FRONT EVAPORATOR TEMPERATURE 3	OVER TEMPERATURE CONTROLLER	0-1000°C	TE407	TC, K	>810°C
FRONT EVAPORATOR TEMPERATURE 4	OVER TEMPERATURE CONTROLLER	0-1000°C	TE408	TC, K	>810°C
REAR EVAPORATOR TEMPERATURE 1	DAS	0-1000°C	TE409	TC, K	
REAR EVAPORATOR TEMPERATURE 2	DAS	0-1000°C	TE410	TC, K	
REAR EVAPORATOR TEMPERATURE 3	DAS	0-1000°C	TE411	TC, K	
REAR EVAPORATOR TEMPERATURE 4	DAS	0-1000°C	TE412	TC, K	

Table 1. STM4-120 Instrumentation and Controls (Continued)

SYSTEM: ENGINE PARAMETER	SIGNAL DESTINATION	OPERATING RANGE	SYMBOL	TYPE	EMERGENCY SHUTDOWN LIMIT
REAR EVAPORATOR TEMPERATURE 1	ECU	0-1000°C	TE413	TC, K	>810°C
REAR EVAPORATOR TEMPERATURE 2	ECU	0-1000°C	TE414	TC, K	>810°C
REAR EVAPORATOR TEMPERATURE 3	ECU	0-1000°C	TE415	TC, K	>810°C
REAR EVAPORATOR TEMPERATURE 4	ECU	0-1000°C	TE416	TC, K	>810°C
FLUE GAS TEMPERATURE	DAS	0-1000°C	TE417	TC, K	
PROPANE MASS FLOW 1	DAS	0-50 SLPM	FT411	FLOW TRANSDUCER	
PROPANE MASS FLOW 2	DAS	0-50 SLPM	FT412	FLOW TRANSDUCER	
PROPANE MASS FLOW 3	DAS	0-50 SLPM	FT413	FLOW TRANSDUCER	
PROPANE MASS FLOW 4	DAS	0-50 SLPM	FT414	FLOW TRANSDUCER	
AIR MASS FLOW 1	DAS	0-50 SCFM	FT421	FLOW TRANSDUCER	
AIR MASS FLOW 2	DAS	0-50 SCFM	FT422	FLOW TRANSDUCER	
AIR MASS FLOW 3	DAS	0-50 SCFM	FT423	FLOW TRANSDUCER	
AIR MASS FLOW 4	DAS	0-50 SCFM	FT424	FLOW TRANSDUCER	
PROPANE FLOW	DAS	0-7.5 ACFM	FT401	FLOW TRANSDUCER	
PROPANE PRESSURE	DAS	0-150 IN H_2O	PT402	PRESSURE TRANSDUCER	
PROPANE TEMPERATURE	DAS	0-100°C	TE418	TC, T	
FLAME 1	DAS	0/24 VDC	BE401	UV SENSOR	
FLAME 2	DAS	0/24 VDC	BE402	UV SENSOR	
FLAME 3	DAS	0/24 VDC	BE403	UV SENSOR	
FLAME 4	DAS	0/24 VDC	BE404	UV SENSOR	
MAIN GAS VALVE ON/OFF	DAS & ECU	0/24 VDC	SV401	NC SOLENOID	OUTPUT FOR SHUTDOWN
BLOWER ON/OFF	DAS & ECU	0/24 VDC	PS401	PRESSURE SWITCH	BLOWER OFF
COOLING WATER TO ENGINE	DAS	0-100°C	TE101	TC, T	
COOLING WATER FROM ENGINE	DAS	0-100°C	TE102	TC, T	
COOLING WATER TO ENGINE/SKID	DAS	0-100°C	TE103	TC, T	
COOLING WATER FROM ENGINE/SKID	DAS	0-100°C	TE104	TC, T	
WATER DT	DAS	0-25°C	TE105	TC, T	
COOLING WATER FROM ENGINE	ECU	0-100°C	TE106	TC, K	>60°C
COOLING WATER TO ENGINE (HX VALVE)	VALVE CONTROLLER	0-100°C	TE107	TC, T	
COOLING WATER TO ENGINE (HX VALVE)	DAS	0-100°C	TE108	TC, T	
COOLING WATER TO ENGINE/SKID	DPM	0-100°C	TE109	TC, T	
COOLING WATER FROM ENGINE/SKID	DPM	0-100°C	TE110	TC, T	
COOLING WATER FLOW FOR ENGINE	DAS & ECU	0-409 LPM	FT101	FLOW TRANSDUCER	<114 LPM
COOLANT WATER VALVE POSITION	DAS	0-1mA	ZT101	POSITION FEEDBACK	
DYNAMOMETER COOLING FLOW SWITCH	DAS & ECU	0-24 VDC	FS201	FLOW SWITCH	NO FLOW (<21.61 LPM)
DYNAMOMETER WATER OUTLET TEMPERATURE	DAS	0-100°C	TE201	TC, K	
DYNAMOMETER WATER OUTLET TEMPERATURE	ECU	0-100°C	TE202	TC, K	>60°C
OIL COOLER WATER INLET	DAS	0-100°C	TE111	TC, K	
OIL COOLER WATER OUTLET	DAS	0-100°C	TE112	TC, K	

Notes: DAS = Data Acquisition System
ECU = Engine Control Unit
DPM = Digital Panel Meter

EMERGENCY CONTROL UNIT

Many of the channels read by the DAS are also read by an emergency control unit (ECU). The ECU monitors critical parameters and will shut down the engine if any parameter is beyond its preset limit. (See Power Control and System Protection.)

SAFETY CONSIDERATIONS

Because the STM4-120 engine is under development, there are many safety considerations. These include high pressures, high temperatures, sodium metal, rotating machinery, and electrical power. Each of these potential dangers is discussed below.

High Pressures

Pressure safety was considered in great detail. The crankcase is pressurized to the mean cycle pressure, a maximum of 12 MPa, making it a pressure vessel. An extensive pressure safety analysis was performed to consider effects on personnel and building damage from pressure waves and fragments if the crankcase were to fail.

The effective volume of the crankcase is about 9 liters without oil, or about 6 liters with engine oil. The crankcase was pressure tested to 16.5 MPa and has a safety factor of 3.0 based on an ultimate strength of 810 MPa for 4140 steel. However, a safety factor of 4.0 is needed to comply with ASME and SNL pressure safety regulations.

An analysis was performed to design a blast shield to be placed over the pressure hull to contain an overpressure wave. The results of the analysis indicated that a 1/4-in. plate with an ultimate strength of 1380 MPa (200 ksi) or a 1-in. plate with an ultimate strength of 414 MPa (60 ksi) would be required to survive the overpressure.

Initially, a safety shield from 1/4-in. 4140 steel was fabricated with the intention of heat treating the shield to 1380 MPa. However, there were no local shops that could heat treat a piece that large. Nevertheless, the safety shield was installed to keep fragments from striking personnel in front of the test cell doors or other objects in the test cell. Calculations were performed and verified that the present shield was more than adequate for fragment containment. Also, another independent analysis was performed to consider the effect of a pressure wave blast without containment. The walls of the test cell are concrete masonry units, reinforced with rebar and the cells filled with concrete. The results of the analysis indicated that the overpressures and impulses would not damage the walls or the window (two 1/4-in. tempered glass panes with a vinyl interlayer between them), but the window frame was not adequately attached to the masonry. Therefore, the window frame was reinforced by welding another frame to the existing frame and anchoring the new frame to the block wall.

The heater heads posed a similar problem, although the total volume of gas in one cycle is only about 0.5 l. The heater heads were pressure tested, but not to 1.5 times the maximum working pressure. The pressure test was not performed due to the stress distribution resulting from the temperature gradient and internal pressure at normal operating conditions. Pressure testing the heater heads alone at room temperature would give a completely different stress distribution. Also, the heater heads have a safety factor of less than 4.0 at 12 MPa. Therefore, another safety shield, although less massive than the one for the pressure hull, would be required to cover the heater head area. Testing the STM4-120 heater heads at operating conditions is not an isolated case. All Stirling engines are faced with the similar situation when testing.

In addition, the evaporators and heater pipes had not been thoroughly tested at high loads. STM personnel recommended continous inspection of evaporator fins through the viewports in the combustors. The inspection was considered necessary to locate "hot spots," which indicate a sodium dry-out condition in the evaporators. If a dryout does occur, the gas supply must be shut off quickly to avoid melting the evaporator.

To resolve all of the above problems, a decision was made to eliminate any need to be in the test cell. This resulted in the installation of a video system to observe the evaporator fins. Four video cameras were mounted 1 m from the combustor viewports. The video signals were routed into the control room where all four signals were sent to a "quad splitter," which allows all four signals to be displayed on a single monitor.

As noted in the finite element analysis section, the pressure hull and oil sump are being redesigned for a safety factor of 4.0, eliminating the need for a safety shield. In the case of the heater heads, the small helium volume reduces the pressure hazard while the insulating housing provides additional protection.

High Temperatures

The heat pipes reach temperatures in excess of 800°C. Most of the hot surfaces are insulated and not exposed, but sections of the combustors are exposed. After opening the gas valves, no personnel are required in the test cell. The ECU monitors nearly every temperature and will initiate a shutdown if any temperature is out of its operating range. All temperatures can be monitored with the DAS, and some critical temperatures are also displayed on panel meters.

Sodium Metal

Sodium is a highly reactive metal. If sodium comes in contact with water, the reaction produces sodium oxides, hydrogen, and heat. The heat can cause the hydrogen gas to ignite and explode. In addition, the sodium oxide can react with moisture in the air, producing sodium hydroxide, a caustic lye. To reduce the danger, open water containers are not allowed in the test cell, and the sprinkler system and safety shower are shut off and drained. Also, the exhaust fan is run during all testing, drawing fresh air into the test cell.

A Na-X fire extinguisher, dry Na-x powder, and a shovel are kept just inside the test cell doors. Other safety equipment, such as goggles, face shields, fire-retardant coveralls, and gloves are available in the ETF.

Rotating Machinery

The STM4-120 engine runs at 1800 rpm, but all rotating machinery is contained within the pressure hull. The dynamometer is also self-contained. The driveshaft connecting the engine to the dynamometer is contained in a safety shield mounted on the dynamometer.

Electrical Power

The test cell contains 480, 208, and 110 VAC power to run the pumps, blower, motor, instrumentation amplifiers, etc. All power is properly terminated and fused. Breakers are open except during testing.

Typical Engine Operation in Test Cell

Although Stirling cycle engine analysis is quite complex, the engine basically produces shaft power in the following manner. Each heat pipe assembly is a propane-fired combustor that transfers heat to an internal-finned evaporator containing sodium. The vaporized sodium, having a higher vapor pressure in the evaporator, travels up to the engine heater head, which contains a tube and shell heat exchanger. The sodium condenses on the tube bundle, transferring its latent heat to the working gas (helium) flowing inside the tubes. The heat causes the working gas to expand and drive the piston. The power generated by the engine is absorbed and measured by an eddy-current dynamometer.

A typical run consists of the following steps. All the safety shutdowns, setpoints, and operating parameters are set to a reasonable start up level. The engine pressure in both the cycle and crankcase is set to the desired mean working pressure. The electric motor is activated and lube oil pressure is verified. The combustor blower is started; however, the purge cycle timer prevents further operation until the system is free of propane. The start burner switch is depressed, the vent valve is closed, and the main and blocking gas valves are opened. The ignition transformers provide the high voltage to the spark plugs in the combustors. The fuel and air valves remain in the "idle" position until the evaporator temperatures reach 500°C. Then the PID controllers "ramp" the temperatures to 760°C in 10 minutes. When the lowest evaporator temperature reaches 760°C, the piston stroke is increased to about 20 mm from 5mm, the electric motor is dropped out of the system, and the engine speed is controlled at 1000 rpm. At this point, the engine is producing less than 1 kW of power. Then the engine speed is increased to 1800 rpm, the evaporator setpoint temperatures are gradually stepped up to 780°C, and the stroke is increased to the full 48.5 mm. To shut down the engine, the main gas valve is closed and the piston stroke is set to zero. The engine cooling water is run until the heater head temperatures are all below 200°C.

Power Control and System Protection

The control system regulates the engine's operating power level and protects the system when operating limits are exceeded. The control system is independent of the DAS, but the control and DAS do share several transducers. Many control functions are carried out by software operations to add flexibility to the controls. The control system also uses hardware limits on operating parameters such as engine speed and evaporator temperatures to provide faster response times.

Developing engine power control procedures is one of the main objectives of the current program. Five variables are available for controlling the output power level of the STM4-120: the heater head temperature, the cooling water temperature, the length of piston stroke, the engine operating pressure, and the engine speed. Under the present testing program, only the first four variables are controlled while the engine is operating. The engine speed is maintained at a constant 1800 rpm.

The power that the STM4-120 engine extracts from the heat pipes is a function of the length of piston stroke. An increase in stroke causes more power to be extracted from the heat pipes, while a decrease in stroke reduces the demand on the heat pipes. A schematic of the system that alters the piston stroke is shown in Figure 24. As discussed earlier, the stroke is changed by tilting the rotating swashplate on which the piston rods travel. Tilting of the swashplate relative to the drive shaft is accomplished with a hydraulic actuator. The direction of the actuator motion is determined by the position of a spool in the hydraulic control valve. Two coils, A and B, position the spool in the valve. If coil B is energized and coil A is neutral, the

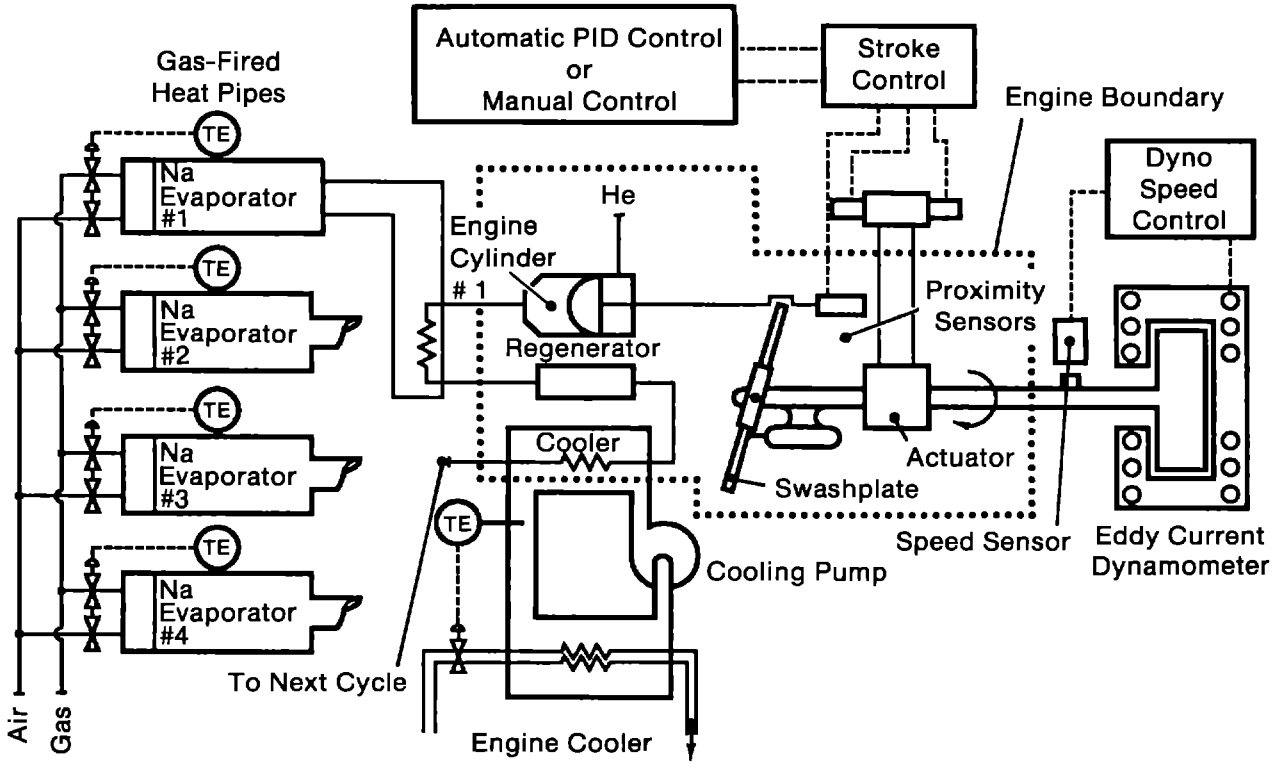

Figure 24. Schematic of control system.

swashplate is driven to a maximum tilt of 22°, producing a 48.5-mm piston stroke. Similarly, if A is energized and B is neutral, the swashplate is driven to zero tilt angle (zero piston stroke). Coils A and B maybe energized simultaneously, causing the stoke to fall between 0° and 22°. Coils A and B are energized with a commercial valve control card that compares a 0-to-10-VDC command signal with the feedback signal on the spool position.

The piston stroke resulting from the control valve actions is measured using two proximity sensors. One sensor is mounted on the shaft, and the other sensor is mounted on the actuator housing. The tilt of the swashplate is determined from the elapsed time between signals from the two sensors. The engine speed is determined by measuring the frequency of pulses from one of the proximity sensors. To produce an error signal for the stroke feedback control, the measured stroke signal is subtracted from the stroke command signal in a simple analog summing junction. This error signal is processed and delivered to the valve control card to correct the tilt of the swashplate.

During initial testing, the power control system will be used to drive the pistons to a selected stroke length, and then maintain the fixed stroke length throughout a series of performance tests. In the performance mapping tests, temperatures in the heat pipe evaporator fins will be regulated by the combustion control system. In the later phases of testing, the power control system will be used to regulate the evaporator temperature by actively controlling the stroke length. Increasing the length of piston stroke will draw more energy out of the heat pipe and cool the evaporator. Similarly, shortening the stroke length will draw less energy out of the heat pipe. This mechanism of power control will more closely simulate the operating mode of the engine when it is tested with a solar concentrator.

In addition to the power control responsibilities of the ECU, the system is also used to coordinate the engine's response to the actions of the auxiliary systems. For instance, if power is lost to the dynamometer, the ECU will close the main gas valve and drive the piston stroke to zero to prevent the engine from over-speeding. Table 1 also lists other circumstances that will cause the ECU to shut down the system. In all these cases, engine testing will be stopped by shutting off the main gas valve and driving the stroke to zero.

V. TEST PLAN

Testing of the STM4-120 will be conducted under three phases. Each phase is a progression toward on-sun testing of the STM4-120 with a reflux solar receiver on Sandia's Test Bed Concentrator. The test plan is divided as follows:

Phase I - Performance Evaluation

During the first 200 hours, the performance of the STM4-120 engine will be determined for various operating conditions. Power and efficiency will be the main concern with respect to operating temperature, cooling fluid temperature, mean cycle pressure, and piston stroke.

Phase II - Full Power Test

For the next 200 hours the engine will be operated at full power. These 200 hours will basically be an endurance test to verify that the engine is in sound working condition. All problems that occur will be documented. Power and efficiency will also be monitored.

Phase III - Performance in Response to Variable Energy Input (Optional)

To determine the responsiveness of the Stirling engine and controls, 100 hours of simulated solar energy input will be used. This will consist of operating the combustion system to increase or decrease the energy input to the engine simulating a typical day. Cloud transients will be emulated in the daily insolation variation.

In addition to evaluating the engine under varying heat input, operating strategies for on-sun testing of the engine will be developed. These will include:

- Start-up: Monitoring to determine whether the sodium in the heat pipes needs to be molten before applying full heat and what gradual increase in temperature, if any, is required.
- Starting: Assessing whether the engine can be motored with the induction generator or whether a separate starter will be required.
- Transients: Determining how the engine will behave during momentary cloud cover; how long it will operate with residual heat from the receiver; whether it can be brought back on-sun immediately afterward.
- Monitoring: Determining which parameters of the engine must be monitored to control the system for operation and emergency shutdown.

Preliminary Test Results

Since its installation in the ETF test cell, the Stirling Thermal Motors kinematic Stirling engine, STM4-120, has operated a total of 181 hours. During this time, the engine cycle pressure was increased from 4 to 10 MPa. At a cycle pressure of 10 MPa, evaporator temperature of 780°C (Sandia has chosen temporarily to operate the engine at 780°C), cooling water temperature of 34°C, engine speed of 1800 rpm, and full piston stroke of 48.5 mm, the engine produced 18.9 kW of peak shaft power at a peak efficiency of 40.1%. A continous shaft power of 14.5 kW at an efficiency of 39.0% has been obtained under similar operating conditions. Figure 25 indicates number of hours at each power level. During a typical test run, the following system parameters are monitored: front and rear evaporator temperatures, heater head temperatures, power output, duct temperature, cycle pressure, and engine efficiency (see Figure 26). The progress made during the past year in the power output with the increased cycle pressure is shown (Figure 27) along with the predicted engine power output from STM's computer code and the GLIMPS©* computer code run at SNL. (GLIMPS provided integrated pressure-volume (PV) power output predictions. The PV power was corrected for piston ring and mechanical losses, based on information from STM, resulting in the shaft power.)

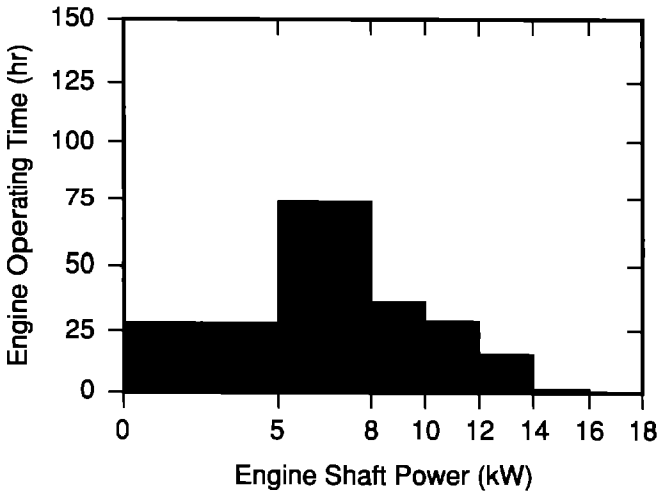

Figure 25. Operating hours versus shaft power.

*GLIMPS © is a Stirling cycle simulation code by Gideon Associates.

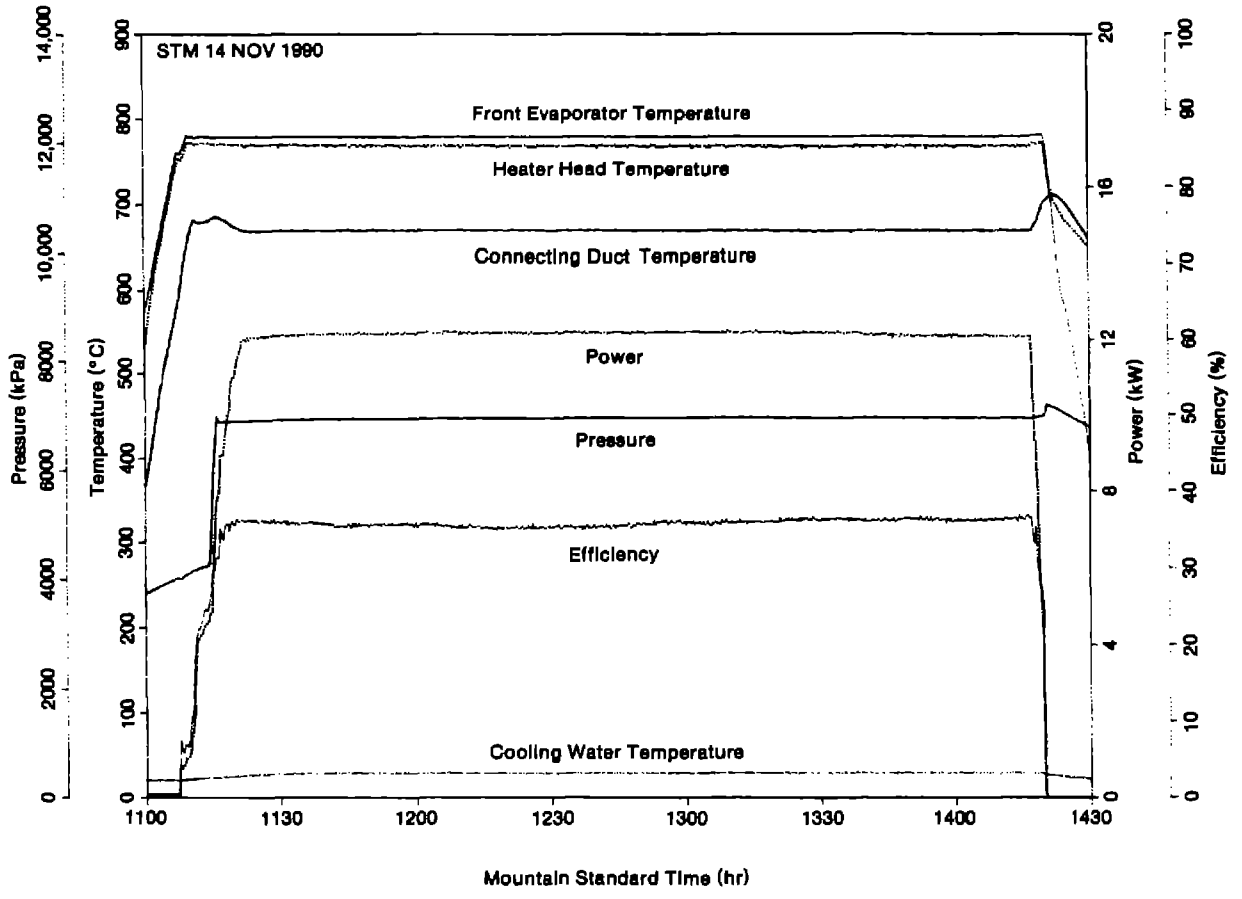

Figure 26. Engine performance.

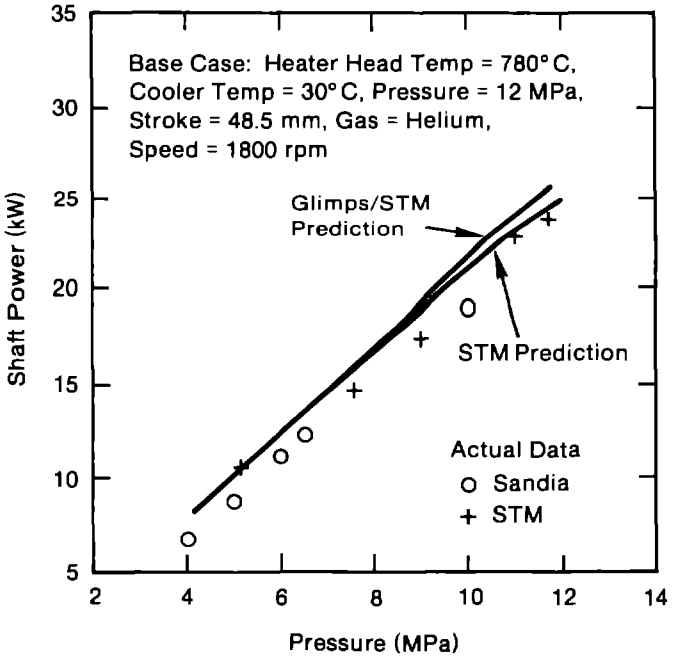

Figure 27. Measured versus predicted performance.

ENGINE

The STM4-120 has performed to mechanical expectations. During initial testing, a potential problem appeared in the original swashplate. Two symmetric cracks developed about the swashplate rotating axis, and an investigation determined that the cracks were a result of an improperly designed drive shaft connecting the engine to the dynamometer. The torsional stiffness of this drive shaft caused the natural frequency, or vibration, of the system to occur near the operating speed of 1800 rpm. Both the drive shaft and the swashplate have since been replaced, without further problems. Mechanical reliability still remains to be verified with further engine testing. After the 500 hours of planned testing, a better determination of the engine's reliability can be made.

HEAT INPUT SYSTEM

During testing, several concerns regarding the heat pipes used to power the Stirling engine have appeared. As a result, the engine shaft power output has been limited to 18.9 kW. The 10-fin, gas-fired heat pipe evaporators (see cutaway area Figure 28) have been the main limitation on the engine's power output [16]. Heat pipe leaks have occurred at the leading edge of the finned evaporators. Investigation has shown that insufficient weld penetration is occurring in the leading edge of the evaporator fins during fabrication.* Without full weld penetration, the combustion gases appear to enter the thin weld areas, causing an internal-to-external oxidation process, resulting in a failure (Figure 29). Because the combustors are operated with 50% excess air, the failure is accelerated by the presence of the additional oxygen. (Fifty percent excess air was recommended by STM to reduce the likelihood of hydrogen diffusion into the heat pipes. Hydrogen causes reduced heat transfer from the sodium vapor to the helium gas. STM has also modified its current heat pipe design to include a hydrogen diffuser to allow excess hydrogen to escape to the atmosphere.)

Other heat pipe failures have occurred at the bellows of the engine's heater heads. The bellows allow for the natural expansion and contraction within the heater head. Metallurgical analysis indicates that the failures are the result of

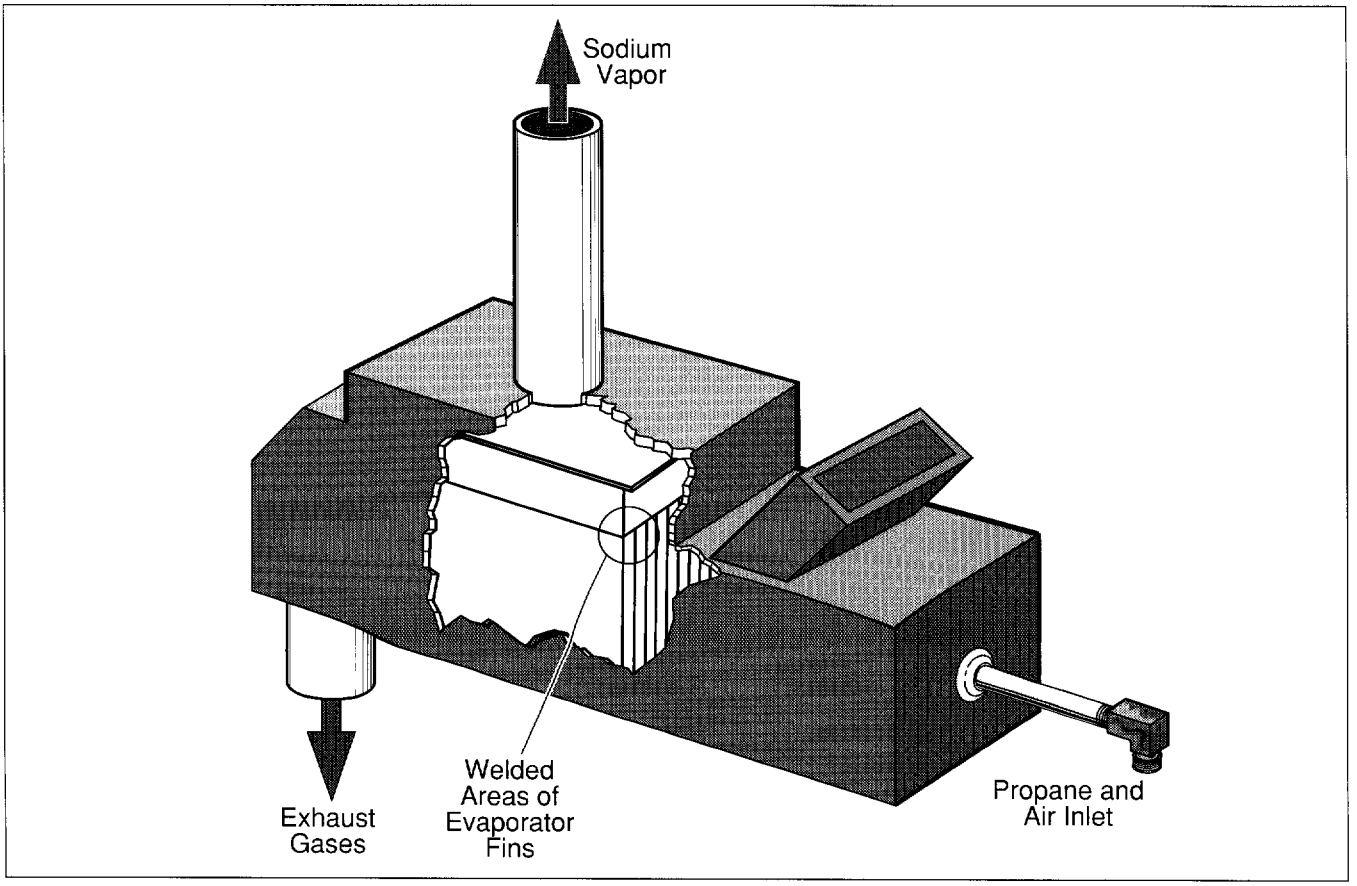

Figure 28. Combustion chamber with cutaway exposing 10-fin evaporator.

*Result of work conducted by Sandia's Mechanical Metallurgical Division.

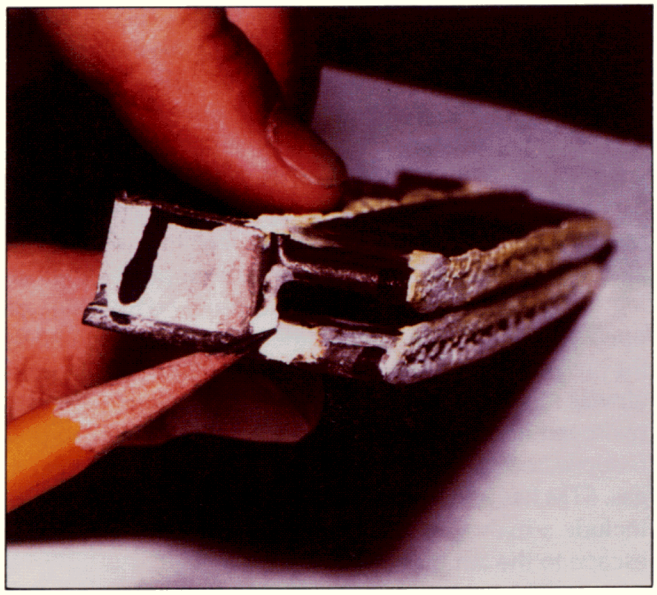

Figure 29. Welded areas of evaporator fins.

external oxidation of the bellows. The outer surface of the bellows (321 SS) oxidized rapidly from the elevated operating temperatures. During normal thermal cycling, the bellows returns to its initial condition, cracking the outer oxidized layer of the material. This layer then flakes off and exposes new, unprotected metal. This process continues during each thermal cycle until a failure occurs. Figure 30 shows a typical bellows from the STM4-120 and two different sections through the bellows. Section A shows how the oxidation propagated through the material thickness and eventually caused a failure. Section B is along a straight section of the bellows where the depth of oxidation is not as severe. Section C shows a curved segment of bellows that has experienced material loss caused by oxidation. (Compare widths of bellows indicated by arrows.) Section D is located at the bellows/regenerator housing interface. This figure shows oxidation migrating through the joint during thermal cycling. Again, an eventual failure would occur. To prevent future failures, all the bellows will be made from Inconel 625, which does not exhibit the rapid oxidation common to SS321. In addition, the 625 provides a fatigue-failure lifetime of 2 million cycles for this bellows design. This compares with SS321, which has a fatigue-failure life of 1000 cycles.* The sections through the bellows also show the absence of sodium attack on the bellows. (The sodium interface is opposite the oxidation side.)

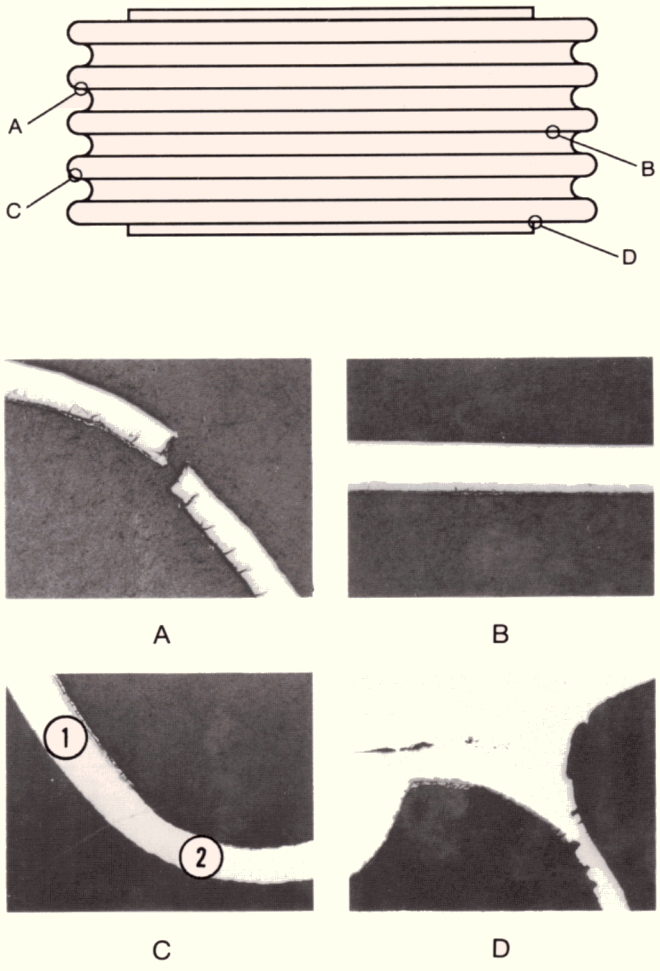

Figure 30. Bellows and sections.

VI. CONCLUSIONS

The STM4-120 has mechanically operated to its design point. Both the powers and efficiencies recorded during preliminary testing have closely followed the design predictions. In fact, engine efficiencies of near 40% have been obtained at half-rated shaft power. Obtaining the designed output power of 25 kW and an efficiency between 42 to 45% should be possible. The present gas-fired heat pipe evaporators have restricted the continued operation of the engine. These units are being reevaluated with alternative methods for providing energy input to the engine. Despite the problems with the gas-fired heat pipe evaporators, valuable experience has been gained. Eventually, a hybrid solar/fossil-fuel-fired receiver will be considered for this engine. The finite element analysis (FEA) conducted on critical engine components provided an additional verification of the STM engine design. All major components exposed to the high temperatures and pressures are designed to meet their functional requirements. With an improved heat input method, testing of the STM4-120 kinematic Stirling engine will continue. Implementing formal testing will be the main thrust during the coming year.

*The fatigue-failure lifetime was calculated by the manufacturer, Metal Bellow.

REFERENCES

1. Ross, A., 1981. *Stirling Cycle Engines*, Solar Engines, Phoenix, AZ.

2. Linker, K.L., 1986. *Heat Engine Development for Solar Thermal Dish-Electric Power Plants,* SAND86-0289, Sandia National Laboratories, Albuquerque, NM.

3. Washom, B.J., 1984. *Vanguard I Solar Parabolic Dish-Stirling Engine Module*, DOE/AL/16333-2, Albuquerque, NM.

4. Droher, J.J., S.E. Squier, and S. Shinnamon, 1986. *Performance of the Vanguard*, EPRI AP-4608, Project 2003-5, Final Report, Energy Technology Engineering Center, Canoga Park, CA.

5. Stearns, J., 1985. *Stirling Engine Alternatives for the Terrestrial Solar Application*, JPL Publication 85-70, DOE/JPL-1060-91, Jet Propulsion Laboratory, Pasadena, CA.

6. Holtz, R.E., and K.L. Uherka, 1988. *A Study of the Reliability of Stirling Engines for Distributed Receiver Systems*, SAND88-7028, Contractor Report, Sandia National Laboratories, Albuquerque, NM.

7. Moreno, J.B., C.E. Andraka, R.B. Diver, W.C. Ginn, V. Dudley, and K. S. Rawlinson, 1990. "Test Results From A Full-Scale Sodium Reflux Pool-Boiler Receiver," *Proceedings of the 12th Annual ASME International Solar Energy Conference,* Miami, FL, April 1990.

8. Diver, R.B., C.E. Andraka, J.B. Moreno, D.R. Adkins, and T.A. Moss, 1990. "Trends in Dish-Stirling Solar Receiver Designs," *Proceedings of the 25th IECEC*, Paper No. 900685, Reno, NV, August 1990.

9. Urieli, I., and D.M. Berchowitz, 1984. *Stirling Cycle Engine Analysis*, Adam Hilger Ltd, Bristol, England.

10. Reader, G.T., and C. Hooper, 1983. *Stirling Engines*, University Press, Cambridge, England.

11. West, C.D., 1986. *Principles and Applications of Stirling Engines*, Van Nostrand Reinhold Publishing Company, New York, NY.

12. Nightingale, N.P., 1986. *The Automotive Stirling Engine Mod II Design Report,* DOE/NASA/0032-28 (NASA CR-175106), NASA - Lewis Research Center, Cleveland, OH.

13. Bhattacharyya, S., 1984. "Creep-Rupture and Fractographic Analysis of Candidate Stirling Engine Superalloys Tested in Air," *Journal of Materials for Energy Systems*, vol. 5, no. 4, pp. 188-204.

14. Cronin, M.J., *Room Temperature Fatigue Properties of Alloy XF-818,* Automotive Stirling Engine Development Program, NASA Contract DEN-3-32.

15. Kister, J., 1989. "Finite Element Analysis of the Heater Head," internal proprietary document by Stirling Thermal Motors, (November, 1989), Ann Arbor, MI.

16. Doebelin, E.O., 1983. *Measurement Systems*, McGraw-Hill Publishing Company, New York, NY.

17. Khalili, K., T.M. Godett, and R.J. Meijer, 1989. "Design and Testing of a Heat Pipe Gas Combustion System for the STM4-120 Stirling Engine," *Proceedings of the 24th IECEC*, Paper No. 899540. Washington, DC, August 1989.

APPENDIX A
System Problems and Solutions

Heat Pipe Sets:

Set #0 = heat pipes with old heater head design
Set #1 = original evaporators with new heater heads (heavier walls)
Set #2 = backup set of heat pipes (new evaporators and heads)

Nomenclature:

CD - Connecting Duct
FE - Front Evaporator
ECU - Emergency Control Unit
DAS - Data Acquisition System
STM - Stirling Thermal Motors

Date	Problem/Action	Cause	Hours
3/17/89	Leak in combustor housing #1 (Set #0).	Hard ignitions (from when combustors lit sequentially instead of simultaneously) blew out insulation.	
3/20/89	CD #4 (Set #0) temperature 200°C low.	Outgassing (only had getters with these heat pipes, no vacuum tubes). Could be a small leak.	1.0
3/24/89	CD #2 (Set #0) temperature 200°C low.	Outgassing or small leak.	
3/30/89	Welded vacuum tubes on #2 and #4 to solve 3/20 and 3/24 problems.	N/A	
3/30/89	Vibration at 1800 rpm.	Improper shaft stiffness.	
4/05/89	CD #2 (Set #0) temperature low.	Outgassing or possible leak.	
4/07/89	CD #3 (Set #0) temperature low.	Leak in vacuum valve. (It was brass!)	
4/11/89	Sent heater heads to STM.	N/A	
5/05/89	Dismantled engine and sent end seal assy to STM for modifications (cast iron sleeve for rear main bearing, harder x-head liners, relocated x-head oil ports, larger oil gallery tubes, end seal lub mod, new one-piece piston, rings, new x-heads for #4 (galled), and #3, new actuator (old actuator seals leaked), new oil sump studs (grade 12.9).	N/A	

5/17/89	New heat pipes (new heater head design) shipped to SNL. Still had brass valves. H_2 diffuser on #1.	N/A	
5/31/89	CD #4 (Set #1) temp low, engine noise.	Outgassing or small leak. New rings not to specifications, flywheel loose.	10.1
6/01/89	Broke rubber coupling on dynamometer driveshaft.	Evidence of melting from heating to remove flywheel.	
6/08/89	CD #4 (Set #1) temperature low.	Outgassing or small leak.	12.5
6/09/89	CD #4 (Set #1) temperature dropping rapidly.	Probable leak.	
6/12/89	CD #4 (Set #1) temperature low.	Probable leak.	
6/21/89	CD #4 (Set #1) temperature low.	Probable leak.	
6/14/89	Fins on #4 (Set #1) very hot, heater head temperature never came up.	Bad vacuum valve (brass valves).	
7/89	Sent heat pipes back to STM to add H_2 diffusers and leak checked all. Added stainless steel valves.		
	Heat pipe #1 (Set #1): Small leak at liquid return in horn cover.		
	Heat pipe #2 (Set #1): No leaks, but a small green spot on bellows/adapter interface.		
	Heat pipe #3 (Set #1): Leak around heater head thermowell (all heater-head thermowells re-welded).		
	Heat pipe #4 (Set #1): No leaks, valve poorly attached.		
	All: new ring welded to burst disk to eliminate crevice.		
8/07/89	Received heat pipes from STM.	N/A	
8/08/89	Installed new piston rings.	N/A	
8/09/89	Hole in heat pipe #3 vacuum tube.	Heated to bend into position, heated too long with torch (spliced in new section).	

8/10/89	RPM oscillated ±200 rpm.	Noise spikes from proximity sensors.	
8/14/89	Overtemp on FE #4 (Set #1).	Leak on liquid return on horn assembly.	23.1
9/26/89	Repaired liquid return cup on all heat pipes. All heat pipes have new horns, CDs, and bellows.	N/A	
10/04/89	Installed repaired heat pipes.	N/A	
10/05/89	CD #4 (Set #1) temperature nosedive.	Pinhole leak in evaporator fin, sixth from left, (previously exposed).	33.2
10/11/89	Received #4 (Set #1 with new evaporator) back from STM with new evaporator.	N/A	
10/16/89	CD #3 (Set #1) rapid temperature drop.	Leak in evaporator #3 - on leading edge of fin on RHS (may be due to previous leaks in brass valves).	43.5
10/16/89	Crack in swashplate in hub section on nut side.	Casting flaw? Resonance problem with original dynamometer shaft?	43.5
11/09/89	New rotating assembly, rear x-head cup holder modified, new end seal, and end seal line orifice modified.	N/A	45.0
11/09/89	New heater head/evaporator assemblies. Performed Residual Gas Analysis on 11/10/89 - no problems.	N/A	45.0
11/28/89	Residual Gas Analysis on heat pipes - small amount of N_2 in heat pipe #3.	N/A	47.0
12/06/89	Residual Gas Analysis on heat pipes. N_2 up one order on heat pipe #1 (Set #2). N_2 up two orders on heat pipe #4 (Set #2).	N/A	61.2
12/18/89	Leak in heat pipe #4 (Set #2) - note 12/06 info, replaced w/ old heat pipe #4.	Leak inward from weld on burst disk.	83.5
12/19/89	Residual Gas Analysis on heat pipes, N_2 up one order on heat pipe #3 (Set #2).	N/A	83.5
1/10/90	New ECU computer/DAS.	N/A	83.9

1/10/90	CD #3 (Set #2) temperature fluctuating. No leak - pumped out H_2. Heat pipe was O.K.	Hydrogen	83.9
1/17/90	CD #1 (Set #2) temperature low.	Leak in bellows - last groove toward block (near braze) at six o'clock position - bellows nearly collapsed.	105.9
1/18/90	Received "newer" heat pipe #4 (repaired burst disk) and "original" heat pipe #3 (new evaporator plus more zirconium) from STM.	N/A	
1/26/90	CD #3 (Set #2) temperature low.	Leak in bellows - last groove (in first convolution) toward block at four o'clock position - bellows nearly collapsed.	113.8
2/27/90	CD #1 (Set #1) temperature low.	Leak in evaporator, (possibly previously exposed - see 7/89).	132.5
9/25/90	Reworked engine and heat pipes received and installed: (1) new ion-nitrided, lubrited, steel x-heads, (2) modified slider cup/piston nut assy, (3) solid A1Aluminum rear crankcase, (4) Inconel 625 bellows.	N/A	132.5
10/04/90	CD #4 (Set #1, Inconel bellows) temperature drop if power > 14 kW.	Leak in evaporator #148, center three fins discolored.	138.5
10/10/90	Dryout on evaporator #4 (Set #2 if power > 14 kW). Also, flame "flickering" around leading edge of fin #8.	Leak in evaporator #152, small leak on leading edge of fin #8.	141.4

DISTRIBUTION:

U.S. Department of Energy (3)
Forrestal Building
Washington, DC 20585
Attn: M. Scheve
S. Gronich
R. Shivers

Bechtel Group, Inc.
MS 50/15
P.O. Box 3965
San Francisco, CA 94119
Attn: B. Lessley

Robert Brown
Hughes Aircraft
Building 805
MS G5
P.O. Box 11337
Tucson, AZ 85734

California Energy Commission
1516 Ninth Street
M-S 43
Sacramento, CA 95814
Attn: A. Jenkins

California Polytechnic University
Department of Mechanical Engineering
Pomona, CA 91768
Attn: W. Stine

Detroit Diesel Corporation
13400 Outer Drive, West
Detroit, MI 48239-4001
Attn: P. Perdue

Electric Power Research Institute
3412 Hillview Avenue
Palo Alto, CA 94303
Attn: E. Demeo

Georgia Power Co. (2)
7 Solar Circle
Shenandoah, GA 30264
Attn: D. Keebaugh
W. King

HGH Enterprises, Inc.
23011 Moulton Parkway
Suite C-13
Laguna Hills, CA 92653
Attn: D. Holl

Lawrence Livermore National Laboratory
University of California
P.O. Box 808, L-122
Livermore, CA 94550
Attn: J. Rittmann

Luz International
924 Westwood Boulevard
Los Angeles, CA 90024
Attn: D. Kearney

Meridian Corporation
4300 King Street
Suite 400
Alexandria, VA 22302-1508
Attn: D. Kumar

NASA Lewis Research Center (2)
21000 Brookpark Road
Cleveland, OH 44135
Attn: R. Shaltens, MS 301-2
J. Dudenhoefer MS 301-2

Pacific Gas and Electric Company (2)
3400 Crow Canyon Road
San Ramon, CA 94583
Attn: J. Iannucci,
G. Braun

Renewable Energy Institute
1001 Connecticut Avenue NW
Suite 719
Washington, DC 20036
Attn: K. Porter

Solar Energy Industries Association (2)
Suite 610
1730 North Lynn Street
Arlington, VA 22209-2009
Attn: C. LaPorta,
S. Sklar

Solar Energy Research Institute
1617 Cole Boulevard
Golden, CO 80401
Attn: B. Gupta

Solar Kinetics, Inc.
P.O. Box 540636
Dallas, TX 75354-0636
Attn: J. Hutchison

Southern California Edison
P.O. Box 800
Rosemead, CA 92807
Attn: C. Lopez

Stirling Thermal Motors, Inc. (10)
275 Metty Drive
Ann Arbor, MI 48103-9444
Attn: T. Godett

University of New Mexico
Department of Mechanical Engineering
Albuquerque, NM 87131
Attn: M. Wilden

Tech. Reps., Inc. (2)
5000 Marble NE
Albuquerque, NM 87110
Attn: J. Stikar

Sandia Internal

3141	S.A. Landenberger (5)
3141-1	C.L. Ward (8) for DOE/OSTI
3151	G.C. Claycomb (3)
3160	J.E. Mitchell
4520	J.A. Leonard
6215	C.P. Cameron, acting
6215	K.S. Rawlinson (10)
6215	G. Smith (5)
6217	P.C. Klimas
8524	J.A. Wackerly
9521	K.L. Linker (10)

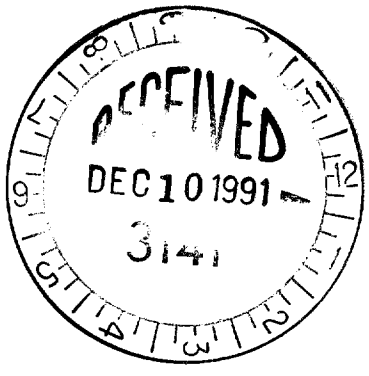
RECEIVED
DEC 10 1991
3141